Three-dimensional simulations of inorganic aerosol distributions in east Asia during spring 2001

Youhua Tang,[1] Gregory R. Carmichael,[1] John H. Seinfeld,[2] Donald Dabdub,[3] Rodney J. Weber,[4] Barry Huebert,[5] Antony D. Clarke,[5] Sergio A. Guazzotti,[6] David A. Sodeman,[6] Kimberly A. Prather,[6] Itsushi Uno,[7] Jung-Hun Woo,[1] James J. Yienger,[1] David G. Streets,[8] Patricia K. Quinn,[9] James E. Johnson,[9] Chul-Han Song,[10] Vicki H. Grassian,[1] Adrian Sandu,[11] Robert W. Talbot,[12] and Jack E. Dibb[12]

Received 1 October 2003; revised 15 February 2004; accepted 24 February 2004; published 25 August 2004.

[1] In this paper, aerosol composition and size distributions in east Asia are simulated using a comprehensive chemical transport model. Three-dimensional aerosol simulations for the TRACE-P and ACE-Asia periods are performed and used to help interpret actual observations. The regional chemical transport model, STEM-2K3, which includes the on-line gas-aerosol thermodynamic module SCAPE II, and explicitly considers chemical aging of dust, is used in the analysis. The model is found to represent many of the important observed features. The Asian outflow during March and April of 2001 is heavily polluted with high aerosol loadings. Under conditions of low dust loading, SO_2 condensation and gas phase ammonia distribution determine the nitrate size and gas-aerosol distributions along air mass trajectories, a situation that is analyzed in detail for two TRACE-P flights. Dust is predicted to alter the partitioning of the semivolatile components between the gas and aerosol phases as well as the size distributions of the secondary aerosol constituents. Calcium in the dust affects the gas-aerosol equilibrium by shifting the equilibrium balance to an anion-limited status, which benefits the uptake of sulfate and nitrate, but reduces the amount of aerosol ammonium. Surface reactions on dust provide an additional mechanism to produce aerosol nitrate and sulfate. The size distribution of dust is shown to be a critical factor in determining the size distribution of secondary aerosols. As much of the dust mass is found in the supermicron mode (70–90%), appreciable amounts of sulfate and nitrate are found in the supermicron particles. For sulfate the observations and the analysis indicate that 10–30% of sulfate is in the supermicron fraction during dust events; in the case of nitrate, more than 80% is found in the supermicron fraction. *INDEX TERMS:* 0335 Atmospheric Composition and Structure: Ion chemistry of the atmosphere (2419, 2427); 0365 Atmospheric Composition and Structure: Troposphere—composition and chemistry; 0368 Atmospheric Composition and Structure: Troposphere—constituent transport and chemistry; 3337 Meteorology and Atmospheric Dynamics: Numerical modeling and data assimilation; *KEYWORDS:* aerosol equilibrium, dust, chemical transport model

Citation: Tang, Y., et al. (2004), Three-dimensional simulations of inorganic aerosol distributions in east Asia during spring 2001, *J. Geophys. Res.*, *109*, D19S23, doi:10.1029/2003JD004201.

[1]Center for Global and Regional Environmental Research, University of Iowa, Iowa City, Iowa, USA.
[2]Departments of Chemical Engineering and Environmental Science and Engineering, California Institute of Technology, Pasadena, California, USA.
[3]Department of Mechanical and Aerospace Engineering, University of California, Irvine, California, USA.
[4]School of Earth and Atmospheric Sciences, Georgia Institute of Technology, Atlanta, Georgia, USA.
[5]School of Ocean and Earth Science and Technology, University of Hawaii, Honolulu, Hawaii, USA.
[6]Department of Chemistry and Biochemistry, University of California, San Diego, California, USA.
[7]Research Institute for Applied Mechanics, Kyushu University, Fukuoka, Japan.
[8]Decision and Information Sciences Division, Argonne National Laboratory, Argonne, Illinois, USA.
[9]Pacific Marine Environmental Laboratory, NOAA, Seattle, Washington, USA.
[10]Department of Environmental Science and Engineering, Gwangju Institute of Science and Technology (GIST), Gwangju, South Korea.
[11]Department of Computer Science, Virginia Polytechnic Institute and State University, Blacksburg, Virginia, USA.
[12]Department of Earth Sciences, University of New Hampshire, Durham, New Hampshire, USA.

0148-0227/04/2003JD004201

1. Introduction

[2] During the springtime, continental outflows in east Asia transport large quantities of aerosols and their precursors over the western Pacific, as indicated by the Transport and Chemical Evolution Over the Pacific (TRACE-P) [*Dibb et al.*, 2003; *Jordan et al.*, 2003a, 2003b; *Clarke et al.*, 2004] and Asian Pacific Regional Aerosol Characterization Experiment (ACE-Asia) [*Huebert et al.*, 2003] observations. The TRACE-P [*Jacob et al.*, 2003] experiment conducted from mid-February to mid-April 2001 was designed to characterize the chemical composition (both gas and aerosol) of the Asian outflow. The ACE-Asia experiment performed from late March to early May 2001 focused specifically on the study of Asian aerosols, with measurements that included detailed aerosol composition as a function of size, as well as optical properties. The aerosol in the east Asia outflow is a complex mixture that contains primary particles arising from diverse sources including: windblown mineral dust; biomass/biofuel burning; sea salt spray; and combustion. The outflow also contains large amounts of secondary particles (e.g., sulfate, nitrate, and ammonium). The TRACE-P and ACE-Asia experiments produced a comprehensive observation-based characterization of the aerosol and its precursors in east Asia.

[3] Inorganic aerosol ions and their equilibrium processes in east Asia have been modeled previously [see, e.g., *Song and Carmichael*, 2001, and references therein]. These studies have found that mineral and sea-salt particles play an important role in determining the quantity and size distribution of inorganic ions. These aerosol (1) provide important reaction surfaces for sulfate production that may increase sulfate production rates by 20 to 80%; (2) play important roles in controlling the partitioning of semivolatile components (such as HNO_3) between the gas and aerosol phases throughout large portions of the troposphere and increase particulate nitrate levels by 10 to 40%; and (3) significantly alter the size distributions of particulate sulfate and nitrate (shifting the distributions to larger particle sizes). These model studies also identified some key issues and uncertainties that could not be resolved/constrained without additional comprehensive observations. These are discussed below along with the new observations provided by the ACE-Asia and TRACE-P experiments:

[4] 1. The particle size distributions of nitrate and sulfate, as well as the relative importance and rates of mass transfer, surface chemistry, and wet and dry removal processes depend critically on the mineral aerosol composition (e.g., calcium content) and how it is distributed as a function of size. Bulk measurements alone are insufficient to constrain models as the above processes are strongly size dependent. The characterization of the nonvolatile aerosol composition as a function of size and location obtained during ACE-Asia and TRACE-P provide critical information upon which to constrain and test model predictions and modules (e.g., mineral dust emissions).

[5] 2. Using present (highly uncertain) estimates of ammonia emissions [*Streets et al.*, 2003], it is estimated that large portions of eastern China should contain both submicron sulfate and nitrate, even during high dust loading conditions. Measurements during ACE-Asia and TRACE-P of size-resolved aerosol chemical composition provide a direct test of this prediction, as well as data to test the emissions and aerosol modules. For example, measurements of aerosol ammonium provide the means to evaluate whether ammonia is a limiting factor.

[6] 3. Strong spatial gradients in aerosol composition as a function of size are expected in the continental outflow regions. Significant horizontal gradients are expected in particulate nitrate and sulfate as dust-laden air mixes with sea salt rich environments. In addition, previous model results suggest strong vertical gradients in aerosol composition/size distributions. For example, carbonate concentrations are often higher in the free troposphere than in the boundary layer. This is true for particles that are lifted rapidly into the free troposphere or are transported over less polluted regions. In either case the carbonate replacement by sulfate and nitrate is slower, so that carbonate is retained longer by the dust particles. Horizontal and vertical gradients measured during the intensive periods by the ship and aircraft platforms provide a test of this finding.

[7] The ACE-Asia and TRACE-P experiments measured aerosol composition using a variety of methods and platforms. Aerosol models provide a tool to help interpret the observed features, and the data provide an excellent opportunity to verify/test model capabilities. During the TRACE-P experiment the aerosol ions were measured by the particle-into-liquid-sampler (PILS) instrument [*Lee et al.*, 2003] on board the NASA P-3B aircraft and the filter method [*Dibb et al.*, 2003] on the NASA DC-8 aircraft. The ACE-Asia C-130 aircraft included more aerosol measurements, including PILS, total aerosol sampler (TAS) [*Huebert et al.*, 2003], and micro-orifice impactor (MOI) [*Huebert et al.*, 2003]. Combining these measurements provides size-resolved aerosol ion information. During the ACE-Asia experiment the CIRPAS Twin-Otter performed aerosol ion observations with an Aerodyne aerosol mass spectrometer (AMS) [*Bahreini et al.*, 2003] around Japan, and the NOAA research vessel *Ronald H. Brown* (RB) provided measurements near the marine surface. These platforms also measured aerosol physical and optical properties.

[8] Data from these experiments are being used to help improve our understanding of Asian aerosols. For example, *Jordan et al.* [2003a, 2003b] discussed the observed aerosol features and their relationship with dust during the TRACE-P experiment. *Tang et al.* [2003a] studied the impact of aerosol and clouds on photolysis frequencies and subsequent influences on regional photochemistry. *Ma et al.* [2003] described the measured aerosol ions associated with biomass burning (BB) air masses. *Tang et al.* [2003b] used a three-dimensional model to simulate BB plumes, and to study the influences on aerosol single scattering albedo (SSA) and gaseous species. Dust storms are a significant source of aerosol during the ACE-Asia period, which is described by both models [*Gong et al.*, 2003; *Tang et al.*, 2004a; *Chin et al.*, 2003] and observations [*Huebert et al.*, 2003]. *Tang et al.* [2004a] studied the effects of the dust heterogeneous reactions and radiative efforts on gas-phase species. The impact of the Asian aerosol on radiative forcing has been studied by *Conant et al.* [2003].

[9] In this paper, we further study the aerosol composition and size distributions in east Asia through the use of a comprehensive chemical transport model. Three-dimensional

aerosol simulations for the TRACE-P and ACE-Asia periods are performed and used to help interpret the observations, with emphasis on the issues outlined above. This paper also discusses various factors that influence the aerosol composition and distribution in the east Asia outflow. In addition, model results are compared with observations in order to evaluate the extent to which this three-dimensional chemical transport model with state-of-the-art treatments of inorganic aerosol equilibria and heterogeneous aerosol chemistry is capable of representing key features of the observations. Finally we discuss improvements in models and measurements needed to enhance our ability to predict aerosol composition and size distributions in the east Asian outflow.

2. Model Description

[10] The regional chemical transport model, STEM-2K3, developed from STEM-2K1 [*Tang et al.*, 2003a; *Carmichael et al.*, 2003a] by adding an on-line aerosol thermodynamics module SCAPE II (Simulating Composition of Atmospheric Particles at Equilibrium) [*Kim et al.*, 1993a, 1993b; *Kim and Seinfeld*, 1995] was used in this study. SCAPE II is a thermodynamics module for calculating gas-particle equilibrium concentrations among inorganic aerosol ions and their gaseous precursors. Particle growth by condensation of water and other trace gases was also considered. Homogeneous nucleation in SCAPE II is predicted to occur when H_2SO_4 concentrations exceed a threshold value

$$C_{crit} = 0.16 \exp(0.1T - 0.035RH - 27.7),$$

where C_{crit} is in units of $\mu g/m^3$, T is temperature in K, and RH is relative humidity in percentage. Here we assumed that all nucleated H_2SO_4 contributes mass to the finest size-bin. For this study, we included aerosols in 4 size bins (in diameter): 0.1 μm–0.3 μm, 0.3 μm–1.0 μm, 1.0 μm–2.5 μm, and 2.5 μm–10 μm, (referred to as bins one to four, respectively). The sum of the first and second bins is directly comparable to observed submicron ions. In this paper only inorganic aerosol species were considered, and the simulated aerosol ions include SO_4^{2-} (sulfate), NH_4^+ (ammonium), NO_3^- (nitrate), Cl^- (chloride), Na^+ (sodium), K^+ (potassium), Ca^{2+} (calcium), Mg^{2+} (magnesium), and CO_3^{2-} (carbonate). Aerosol growth due to coagulation was considered for bins 1–2 (accumulation mode) based on *Whitby* [1978].

[11] The three-dimensional model covers east Asia with 80 km horizontal resolution. RAMS meteorological model provided the meteorological field. Gas-phase chemistry was simulated by the atmospheric chemical mechanism SAPRC99 [*Carter*, 2000]. Lateral boundary conditions for gases and aerosol ions were based on aircraft profiles measured in the TRACE-P and ACE-Asia experiments. Since very strong sources existed near the surface of our model domain, the lateral boundary conditions have relatively weak influences at low altitudes. Complete details of the model setup are presented by *Tang et al.* [2003a] and *Carmichael et al.* [2003a]. The on-line SCAPE module was optimized to reduce the computer time in the STEM-2K3 framework. In the simulations presented here the SCAPE module was called every hour to calculate the aerosol composition for each grid with an ambient relative humidity (RH) greater than 30%. (If the RH is lower than 30%, we assume equilibrium exchange is less important.) To accommodate the four-bin SCAPE module, STEM-2K3 was extended to treat size-resolved primary aerosols. Dust and sea salt were emitted into all four bins, while primary black carbon (BC) and organic carbon (OC) entered the smallest two bins (diameter < 1.0 μm). The on-line TUV photolysis and optical depth calculations [*Tang et al.*, 2003a] were also modified to explicitly account for the radiative impacts of size-resolved aerosols. Aerosol optical properties calculated from the four-bin aerosols are similar to those in previous studies [*Tang et al.*, 2003a; *Conant et al.*, 2003].

2.1. Consideration of Dust

[12] Dust is a major aerosol component in the east Asia outflow during the spring. In order to study the impact of dust on aerosol composition the interactions of dust with ambient air are explicitly treated, taking into account gaseous sorption processes (with saturation effects), and subsequent surface reactions. The composition of dust plays a critical role in determining the importance of these interactions. The composition of the dust used in the calculations was determined using the measurements on board the C-130. The volume concentration of refractory supermicron particles was measured with the thermo-optic aerosol discriminator (TOAD) using an evaporative temperature greater than 300°C [*Clarke et al.*, 2004]. Under high dust conditions the coarse aerosol fraction is assumed to be dominated by dust, and the coarse-particle volumes can be converted to dust mass concentration using an appropriate density [*Clarke et al.*, 2004]. This mass concentration of supermicron dust was found to be strongly correlated with coarse calcium, magnesium, and sodium during the high dust periods (e.g., C-130 flights 6, 7, and 8). These correlations were then used to set the chemical composition of the primary ions of the dust used in this paper. Assuming that the main anion in the emitted dust is CO_3^{2-}, we derived the dust CO_3^{2-} from the observed soluble calcium amount. It was assumed that the original dust emitted into the atmosphere did not contain gypsum [*Mori et al.*, 2003], and that all sulfate associated with the dust surface was produced from interactions with pollutants in the ambient air. The Ca^{2+}, Mg^{2+}, Na^+, and CO_3^{2-} were found to account for 1.14%, 0.116%, 0.153%, and 2.19% of the dust mass, respectively. It is important to emphasize that the values determined in this way exploit the correlation between the dust mass inferred from the volume measurements and the observed soluble calcium mass. The absolute value of the total dust mass was unconstrained by direct measurement. Therefore these results are uncertain (perhaps by a factor of 2). The calcium values estimated in this manner are consistent with those determined from elemental analysis of soils in the dust-source regions east of 100E, where calcium is 1–3% by weight. However, there are some soil regions where calcium accounts for up to 6% of the soil mass. Calcium in surface aerosol measured around the source regions of the Inner Mongolia Autonomous Region were found to range from 1–2% by weight [*Mori et al.*, 2003].

[13] The inorganic aerosol composition was calculated using SCAPE-II assuming that the particles within each size

bin are internally mixed and in equilibrium with the gas phase. However, for the dust rich-periods studied here, it was found that this assumption leads to calculated values that are inconsistent with the observations (e.g., a systematic underprediction of NH_4^+). A similar finding was reported by C. H. Song et al. (Aerosol mixing state inferred from highly time resolved composition measurements and an aerosol thermodynamic model: Case studies from ACE-Asia and TRACE-P, submitted to *Journal of Geophysical Research*, 2003) (hereinafter referred to as Song et al., submitted manuscript, 2003) when analyzing the PILS data using a stand-alone version of SCAPE-II constrained by the observations. Their analysis found that the measurements could be best reproduced by the model when only 30% of the calcium in the dust was assumed to be chemically active and available for equilibrium interactions. Recent microscopy studies (A. Laskin, personal communication) using Chinese soils found that ~10% (by number) of the soil particles contained calcium that completely reacted with nitric and sulfuric acid under laboratory conditions, while another 30% of the particles contained calcium inclusions that did not become hydroscopic when reacted under the same conditions. In addition, a carbonate signature was inferred in aerosols measured on board the C-130 using FTIR by the absorbance remaining after rinsing with hexane, acetone, and water (L. Russel, personal communication). Significant amounts of carbonates remaining in the aged aerosol is also supported by the analysis of the PILS data determined from the difference between the measured cations and anions in the submicron fraction of the aerosol in the east Asia outflow (K. Maxwell-Meier et al., Inorganic composition of particles in mixed dust: Pollution plumes observed from airborne measurements during ACE-Asia, submitted to *Journal of Geophysical Research*, 2003) (hereinafter referred to as Maxwell-Meier et al., submitted manuscript, 2003).

[14] In this study we accounted for these findings by defining the portion of the calcium in the dust that was active for chemical reaction to be 30, 30, 20, and 10% for the four size bins, respectively. Although the dust realistic portion involved in equilibrium process should be varied, the ACE-Asia C-130 measurements indicated that these active ratios could represent the first-order approximation (Song et al., submitted manuscript, 2003) during dust events. The same active ratios were also applied to dust magnesium.

[15] To represent the involvement of dust in heterogeneous chemistry, we define the dust surface fresh ratio as

$$D_{fresh} = \frac{Ca_{active} - CaSO_4 - Ca(NO_3)_2}{Ca_{active}}, \qquad (1)$$

where Ca_{active} is the amount of dust active calcium that is available for heterogeneous chemistry. All ions are in molar units. The amounts of $CaSO_4$ and $Ca(NO_3)_2$ are calculated by the on-line SCAPE model. D_{fresh} is an important ratio, since only that dust calcium not tied up as $CaSO_4$ or $Ca(NO_3)_2$ can be involved in heterogeneous reactions, and its value is a measure of the "chemical" age of the dust. D_{fresh} varies in value from 1 for fresh, unreacted dust, to 0 for completely aged particles.

[16] In this paper, the following heterogeneous reactions on dust surface are considered [*Tang et al.*, 2004a]:

$$O_3 \xrightarrow{\text{Dust}} 1.5O_2$$

$$SO_2 \xrightarrow{\text{Dust}} SO_4^{2-}$$

$$NO_2 \xrightarrow{\text{Dust}} NO_3^-$$

$$HNO_3 \xrightarrow{\text{Dust}} NO_3^-.$$

We assume the uptake coefficients to be size-independent, with values for $\gamma(O_3)$, $\gamma(SO_2)$, $\gamma(NO_2)$ and $\gamma(HNO_3)$ of 5×10^{-5} [*Michel et al.*, 2002; *Dentener et al.*, 1996; *Jacob*, 2000], 1×10^{-4} [*Usher et al.*, 2002; *Zhang and Carmichael*, 1999; *Phadnis and Carmichael*, 2000; *Goodman et al.*, 2001], 1×10^{-4} [*Underwood et al.*, 2001], and 0.01 [*Prince et al.*, 2002; *Goodman et al.*, 2000; *Hanisch and Crowley*, 2001], respectively. The values of the uptake coefficients used here are those determined under dry laboratory conditions with the exception of nitric acid. In the case of nitric acid a deliquescent layer is assumed, corresponding to a higher value (i.e., 0.01). Further details regarding the treatment of the heterogeneous reactions are presented by *Tang et al.* [2004a].

2.2. Emissions

[17] Anthropogenic emissions used in this study were based on *Streets et al.* [2003], and the biomass burning emissions are from *Woo et al.* [2003]. For the purposes of this paper, special emphasis was placed on those emissions that directly impact the aerosol calculations. An evaluation of the gas-phase emissions of SO_2, NO_x, and NMHC (important secondary aerosol precursors) during ACE-Asia and TRACE-P has been discussed elsewhere [*Carmichael et al.*, 2003b]. Emissions of NH_3 play an important role in secondary aerosol formation. As discussed by *Streets et al.* [2003], NH_3 emissions in Asia are dominated by activities associated with livestock and agricultural fertilizer, with the highest emission densities coming from the intense agricultural regions in east China, Japan, and Korea (as shown later in Figure 19). These estimates are highly uncertain (factor of 2). The role of NH_3 in aerosol processes in this region is discussed in more detail in later sections.

[18] The model also treats size-resolved emissions of primary aerosol including dust and sea salt. These emissions were calculated on-line using information provided by the dynamic meteorological model as described in detail by *Tang et al.* [2004a]. In addition, we included the primary emissions of particulate K^+, associated with biofuel/biomass combustion. By analyzing the TRACE-P measurements, we found that potassium was highly correlated with BC (correlation coefficient $R > 0.9$), with a total particulate mass ratio of K^+/BC of 0.43. We used this ratio along with the BC emission estimates from biorelated combustion [*Streets et al.*, 2003] to estimate potassium emissions.

3. Inorganic Aerosol Distributions in East Asian Outflows

[19] Asian aerosol contains large amounts of sulfate, nitrate and ammonium ions, with gradients in the outflow

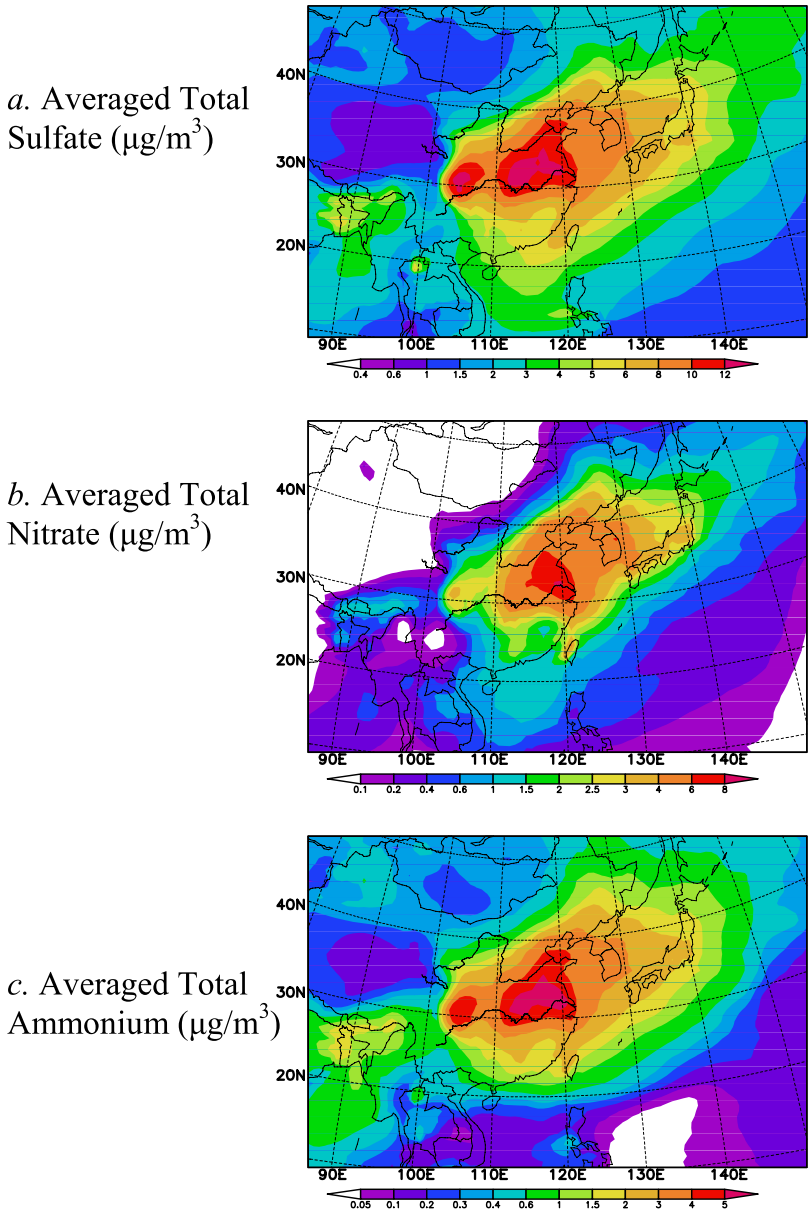

Figure 1. Simulated mean sulfate, nitrate, and ammonium concentrations at 400 m level for March and April.

reflecting the spatial distribution of the NO_x, SO_2, and NH_3 emissions and the positions of the springtime cold fronts as they move out and over the western Pacific. The calculated mean distributions of near surface sulfate, nitrate and ammonium are shown in Figure 1 for March and April. The aerosol distributions of these three components are similar, with the highest aerosol amounts calculated over the source regions, with elevated levels extending out over the Yellow Sea, the Japan Sea, and into the western Pacific above latitudes of 30°N. Throughout most of this region sulfate exceeds nitrate, which reflects in part the fact that anthropogenic sulfur dioxide emissions are significantly higher than nitrogen oxide emissions (by a factor of 3, on a mass basis). Over Taiwan and Japan the relative importance of nitrate aerosol increases. The ammonium spatial distribution is very similar to that for sulfate, which implies that ammonium formation is controlled mainly by sulfate nucleation in this region.

[20] These mean distributions are heavily influenced by the strong outflow events that occur in association with the cold front passages. These frontal events produce strong gradients in the spatial and temporal distributions. The aerosol distributions in the outflow can vary greatly depending on the time of year and location of the cold front. For example frontal events in early spring can contain large amounts of pollution mixed with aerosol from biomass burning in Southeast Asia, while later in spring dust can become significant. The TRACE-P and ACE-Asia experiments sampled this variability. In the following sections, we investigate the aerosol distributions during various outflow conditions. Figures 2a–2i show

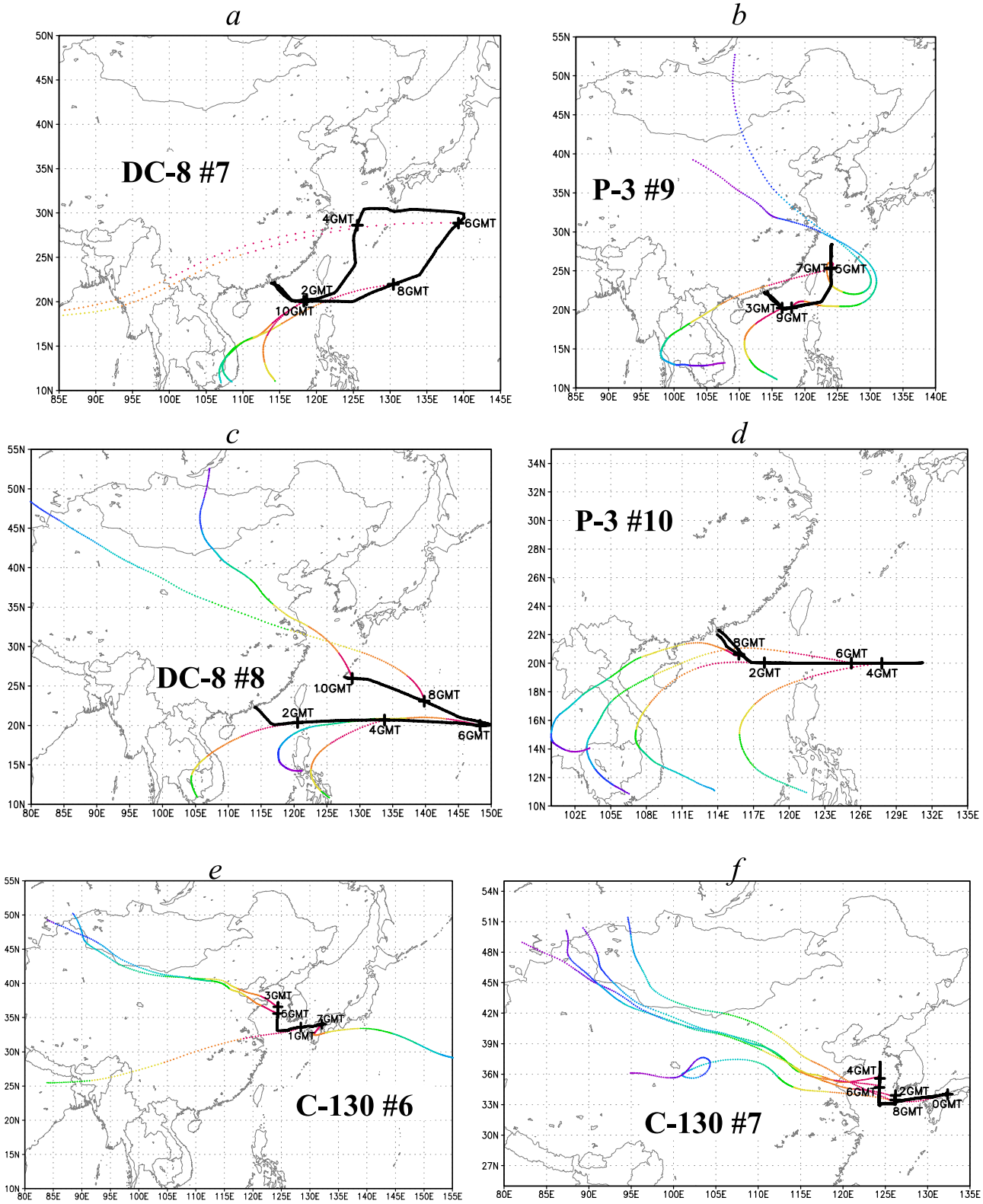

Figure 2. The paths of selected TRACE-P and ACE-Asia flights, and the NOAA R/V *Ronald Brown* (RB) (cruise path marked in Julian day). Trajectories arriving at these paths every 2 hours (2 days for the RB) are colored by day from the arrival point. Trajectories are started at the actual altitudes of the flights at the times indicated, and 500 m above sea level for the ship *Ron-Brown*.

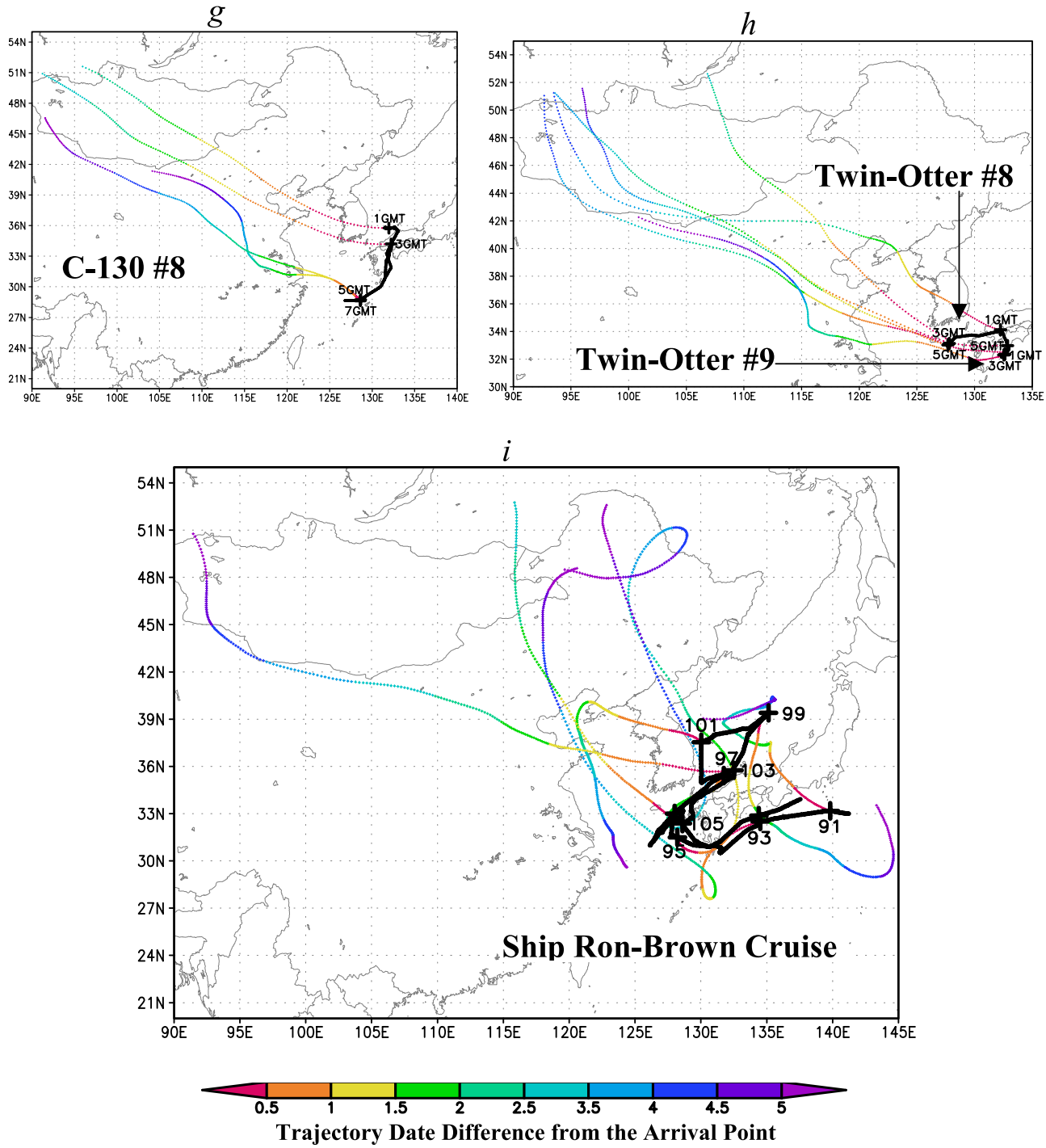

Figure 2. (continued)

selected TRACE-P and ACE-Asia observation periods discussed in this paper.

3.1. Pollution Events

[21] The TRACE-P DC-8 flight 7, P-3 flight 9 (March 7), DC-8 flight 8 and P-3 flight 10 (March 9) sampled typical Asian outflow affected by frontal activities, with contribution from biomass burning. *Carmichael et al.* [2003a] described the Asian outflow pattern in these four flights. *Tang et al.* [2003b] discussed the BB impacts on these flights. In comparison with non-BB air masses, the analysis of *Tang et al.* [2003b] indicated that BB air masses tended to have higher CO and potassium, but lower single scatter albedo due to enhanced levels of black carbon.

3.1.1. DC-8 Flight 7

[22] Figures 3a–3i shows the comparison of simulated carbon monoxide, ethane, sulfate, nitrate, ammonium, potassium, sodium, and magnesium with measurements for the TRACE-P DC-8 flight 7 (see Figures 2a–2i). This flight sampled both prefrontal and postfrontal air masses. The

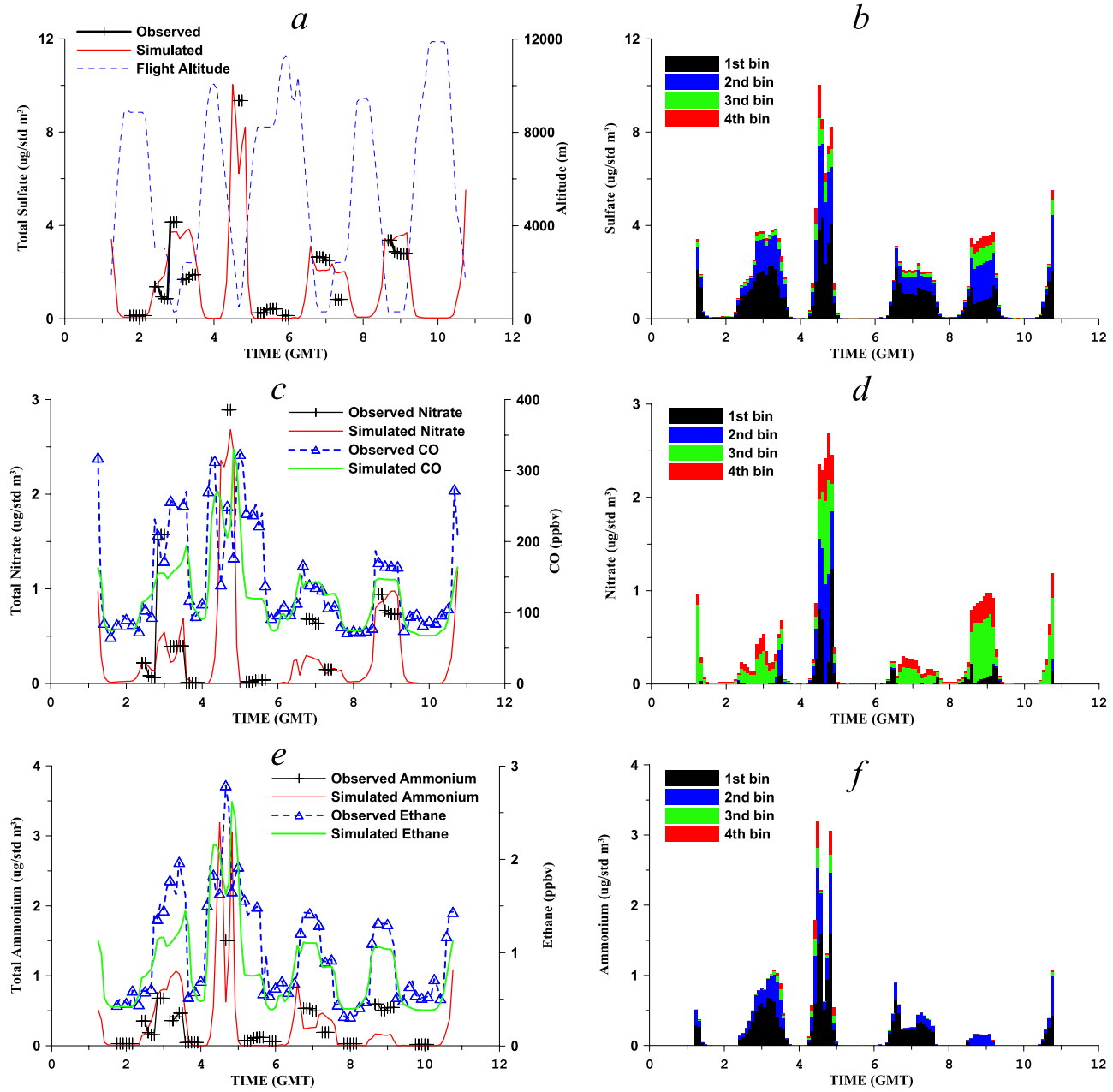

Figure 3. Observed and simulated total sulfate, nitrate, ammonium, potassium, sodium, magnesium, CO, ethane, and relative humidity, and simulated ion size distributions along the path of DC-8 flight 7, March 7, 2001. Plot i shows the vertical profiles of sulfate and its fine ratio for prefrontal (after 6 GMT) and postfrontal (4:30–5:20 GMT) flight segments.

postfrontal air (times <5 GMT) was significantly enhanced in trace gases (e.g., CO and ethane) as well as secondary aerosols including nitrate and sulfate. The predicted aerosol total mass (sum of all four bins) is compared to DC-8 filter measurements [*Jordan et al.*, 2003b] in Figures 3a, 3c, 3e, 3g, and 3h. Both the observations and predictions show that the highest concentrations of ions, as well as gas-phase species, appear between 4–5 GMT at low altitudes (<2 km). The predicted values capture many of the important observed features, but with a tendency to underestimate peak values (e.g., nitrate at 7 GMT).

[23] The aerosol composition and size vary in the prefrontal and postfrontal regions. For example, whereas the total sulfate concentrations are similar for flight segments at 3 GMT (124.24E, 23N) and 9 GMT (124.78E, 20N), the simulated sulfate size distributions at these times are different (Figure 3b). At 3 GMT the submicron particles contain more than 90% of total sulfate mass, while at 9 GMT the fine ratio (the mass of the submicron fraction divided by the total mass) decreased to 0.7.

[24] The size distributions of sulfate and nitrate reflect the role that acid-alkaline balance processes play. In the ion equilibrium system considered here, SO_4^{2-} is the strongest and the only nonvolatile secondary acid ion. If there is insufficient alkaline ion available to neutralize the sulfate, the aerosol system becomes acidic, and volatile anions such

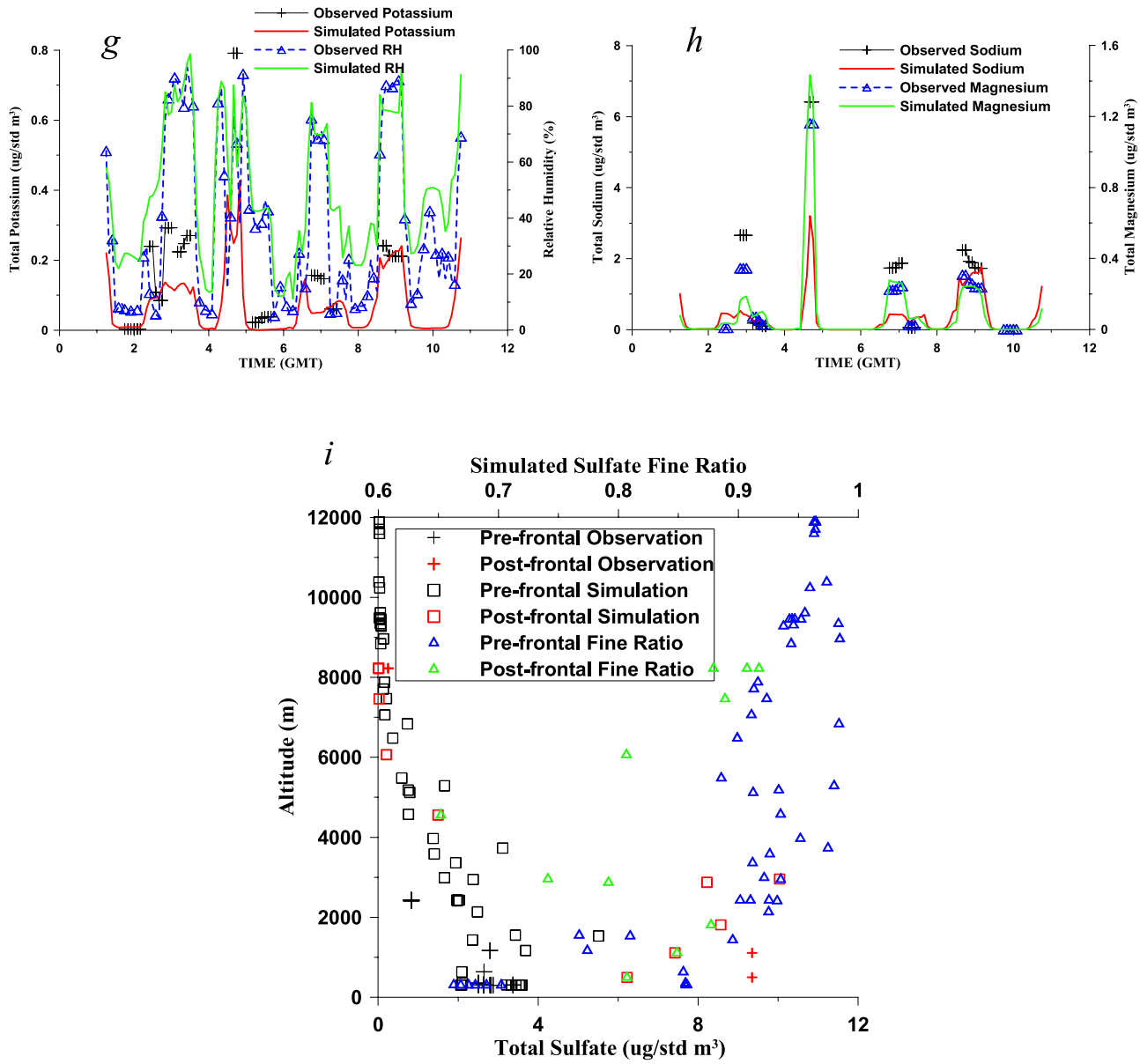

Figure 3. (continued)

as CO_3^{2-}, Cl^-, and NO_3^- are expelled from the aerosol. The acidic system attracts alkaline ions, such as $NH_3 \rightarrow NH_4^+$. In the absence of primary aerosol, such as dust or sea salt, sulfate arises from nucleation processes that produce fine particles that eventually grow into the accumulation mode via coagulation and water uptake. Under these conditions sulfate is usually concentrated in the submicron fraction. Throughout the entire flight, simulated nitrates were concentrated in the 1–2.5 μm size range, where it was associated with sea salt particles through displacement of Cl^- by gaseous HNO_3 (as illustrated by the elevated sea salt Na^+ levels observed (and calculated) during the flight segments in the marine boundary in Figure 3h).

[25] In the equilibrium system considered here NH_4^+ is the only volatile alkaline ion. Figure 3e shows that the simulated total ammonium concentrations generally track the filter measurements. In addition the ammonium size distribution is similar to that of sulfate. As discussed above, there is little submicron nitrate calculated (with the exception of the segment at 4–5 GMT), indicating that for this flight there was an insufficient amount of ammonium to fully neutralize the sulfate. The simulation also shows some skill in predicting metal ions, including potassium, sodium and magnesium (Figures 3g and 3h). For this flight these ions came mainly from sea salt, especially in the low-altitude segments with relatively high relative humidity (RH). The size distribution of these alkaline ions is determined mainly by their emissions, but can be shifted to larger sizes when water uptake occurs.

[26] This flight encountered a cold front around 5 GMT, which significantly influenced pollutant transport [*Carmichael et al.*, 2003a]. Figure 3i shows vertical profiles of sulfate along ascents/descents in the prefrontal and postfrontal regions. Both the measurements and the predic-

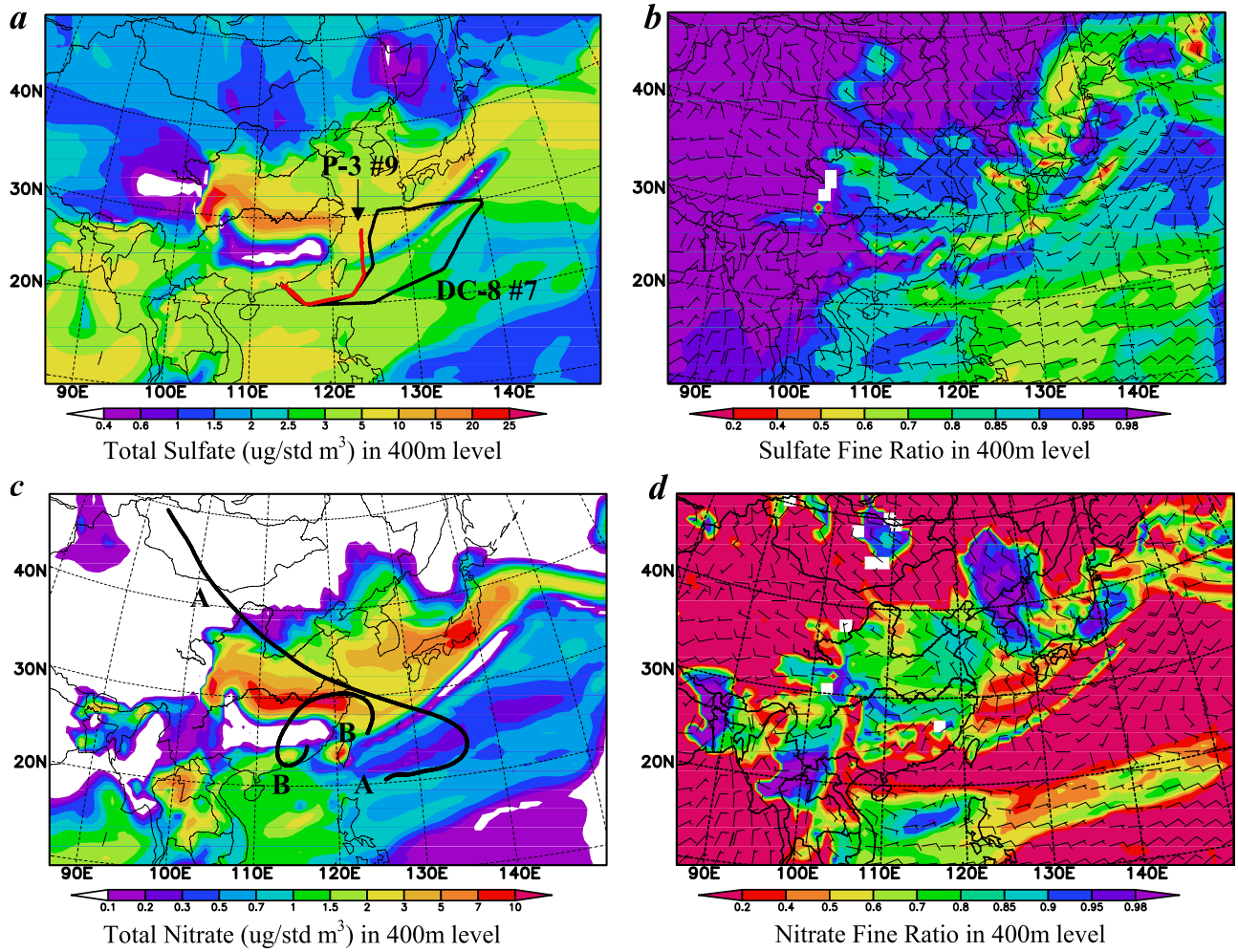

Figure 4. Simulated total sulfate, nitrate, and their fine ratios at 6 GMT, March 7 at 400 m layer. (c) Trajectories that arrived at the DC-8 flight 7 at 8:45 GMT (trajectory A), and the P-3 flight 9 at 6:55 GMT (trajectory B).

tions show that in the prefrontal region the total sulfate concentrations decrease monotonically with increases in altitude, while the fraction of mass in the fine mode increases. In the prefrontal regions, vertical convection is usually not very active, and a larger fraction (in this case about 30%) of the sulfate is in the supermicron modes where it is associated with sea salt. Behind the front the aerosol loadings are higher, and elevated levels of sulfate extend to altitudes up to 6 km. The sulfate fine ratio in the postfrontal region showed a decrease from 2 to 5 km level (Figure 3i), as the result of sea salt particles lifted in the front. Sodium mainly came from sea salt, the simulated sodium agreed well with the measurement (Figure 3h).

[27] Figure 4 shows the horizontal distributions of simulated total aerosol sulfate and nitrate, and their fine ratios at 400 m and 6 GMT, March 7. These distributions illustrate that strong gradients in aerosol size and composition can occur in the Asian outflow, as a result of the flow conditions and the spatial distribution of the sources. The Sichuan basin in China (105E, 30N) has very high SO_2 emissions due to the heavy use of regional sulfur-rich coal. Sulfate concentrations are maximum in this region and are transported to the east in the postfrontal flow. The cold front and its associated rain band resulted in an aerosol-depleted zone that extended from southern China to the east of Japan. Under the influence of this weather system, high nitrate concentrations were produced: along the Yangtze River, where several megacities exist; in a region extending over Korea and Japan; and a region that includes Bangkok. Figures 4b and 4d show that the sulfate and nitrate fine ratios range from 0.5 to 1 over polluted regions. In the prefrontal area the fine fraction decreases for both sulfate and nitrate due to interactions with sea salt. In the postfrontal zones the fine fractions show appreciable variability, with values decreasing due to interactions with mineral dust (e.g., central China) and sea salt (e.g., the Japan and Yellow Seas).

[28] The aircraft in situ measurements reflect the aerosol composition after the air has been transported significant distances from the land (the ages of the air masses sampled from the time they were last impacted by fresh emissions were typically >2 days). The aerosol composition and size depend critically on this air mass history. To illustrate this, we investigated how the aerosol characteristics change along various trajectories. Figure 4c shows two trajectories that arrived at the paths of DC-8 flight 7 at 8:45 GMT and

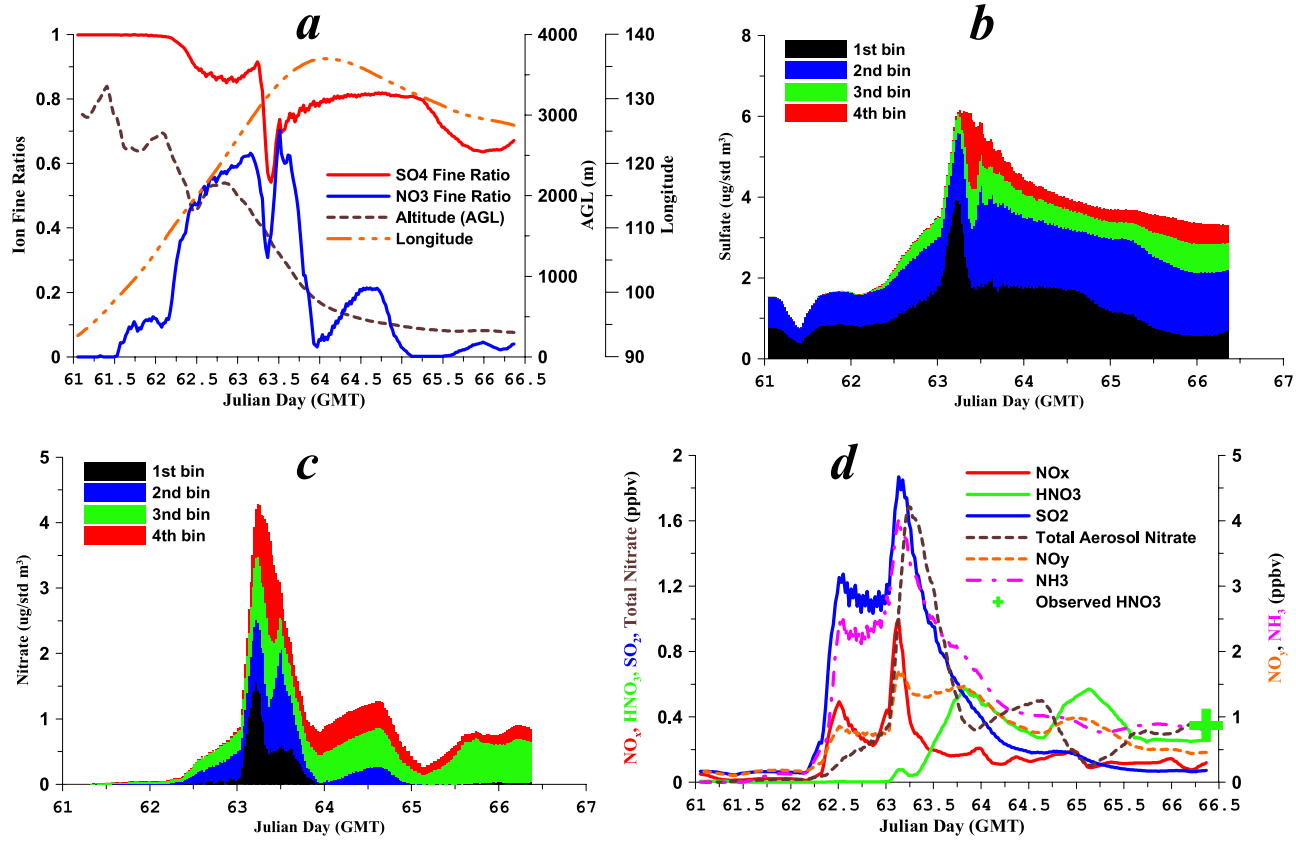

Figure 5. Simulated (a) sulfate and nitrate fine ratios, (b) size distributions of sulfate, and (c) nitrate, and (d) species concentrations of NO_x, HNO_3, SO_2, nitrate, NO_y, and NH_3, along with the trajectory A (Figures 3a–3i).

P-3 flight 9 at 6:55 GMT; these are labeled as trajectories A and B, respectively.

[29] Figure 5 shows the details of trajectory A as well as predictions extracted along the trajectory. The predictions were spatially and temporally interpolated along the trajectory locations from the calculated three-dimensional fields. Four days before the air mass was sampled by the DC-8, trajectory A was over Mongolia at an altitude >3 km. In this region the aerosol was dominated by submicron sulfate, reflecting the widespread use of coal. This air mass descended as it traveled eastward. The aerosol quantities increased when the trajectory reached the eastern provinces of China (115°E at Julian day 62.5), where at an altitude of ~2 km the air mass encountered pollutants mixed with dust (a small dust event occurred during this period). As shown in Figures 5b, 5c, and 5d, gas-phase pollutants, as well as aerosol sulfate and nitrate increased significantly. Some of the aerosol sulfate and nitrate was associated with the windblown dust (calcium in the air mass below 2 km was a few $\mu g/m^3$) as indicated by the increase in mass in the third bin (1–2.5 um). This trajectory passed over Shanghai on Julian day 63.3 (7 GMT, March 4) at an altitude of ~1.5 km. Most emitted pollutants, like SO_2 and NO_x, reached their peaks at this time. Importantly, NH_3 concentrations were predicted to be in excess of 3.5 ppbv throughout this portion of eastern China (reflecting the intense agricultural activity in the region). Over Shanghai the aerosol nitrate reached 2/3 that of sulfate. Over the city there was a distinct enhancement in the smallest sized particles (the first bin), and this was associated with the production of ammonium nitrate and sulfate. It is important to note that both were formed due to the abundance of NH_3.

[30] As the air mass entered the marine boundary layer in the Yellow Sea (between Julian day 63–64), the polluted continental outflow mixed with dust was further modified by interactions with sea salt. The concentrations of sulfate and nitrate in the supermicron fraction increased as secondary aerosols were produced, sulfur oxides and nitric acid interacted with the sea salt and dust surfaces, and the particles grew in the high humidity conditions within the marine boundary layer. These processes are reflected in the changes in the submicron amounts of nitrate and sulfate. Figure 5 shows that the size distributions of nitrate and sulfate behaved differently. Prior to arriving over the polluted regions, sulfate was concentrated in the submicron particles, while nitrate was mostly in the supermicron fraction. In the highly polluted regions, sulfate in the supermicron fraction increased, while that for nitrate decreased. During the rapid transport in the frontal outflow in the marine boundary layer between Julian day 63 and 64 the size distribution of nitrate changed dramatically. During this period nitrate in the finest mode decreased, while that in the second bin increased. This is the result of both particle growth, and the increased acidity of the aerosol due to interactions with sulfate. The release of nitrate from the aerosol to the gas phase as the aerosol acidifies can be

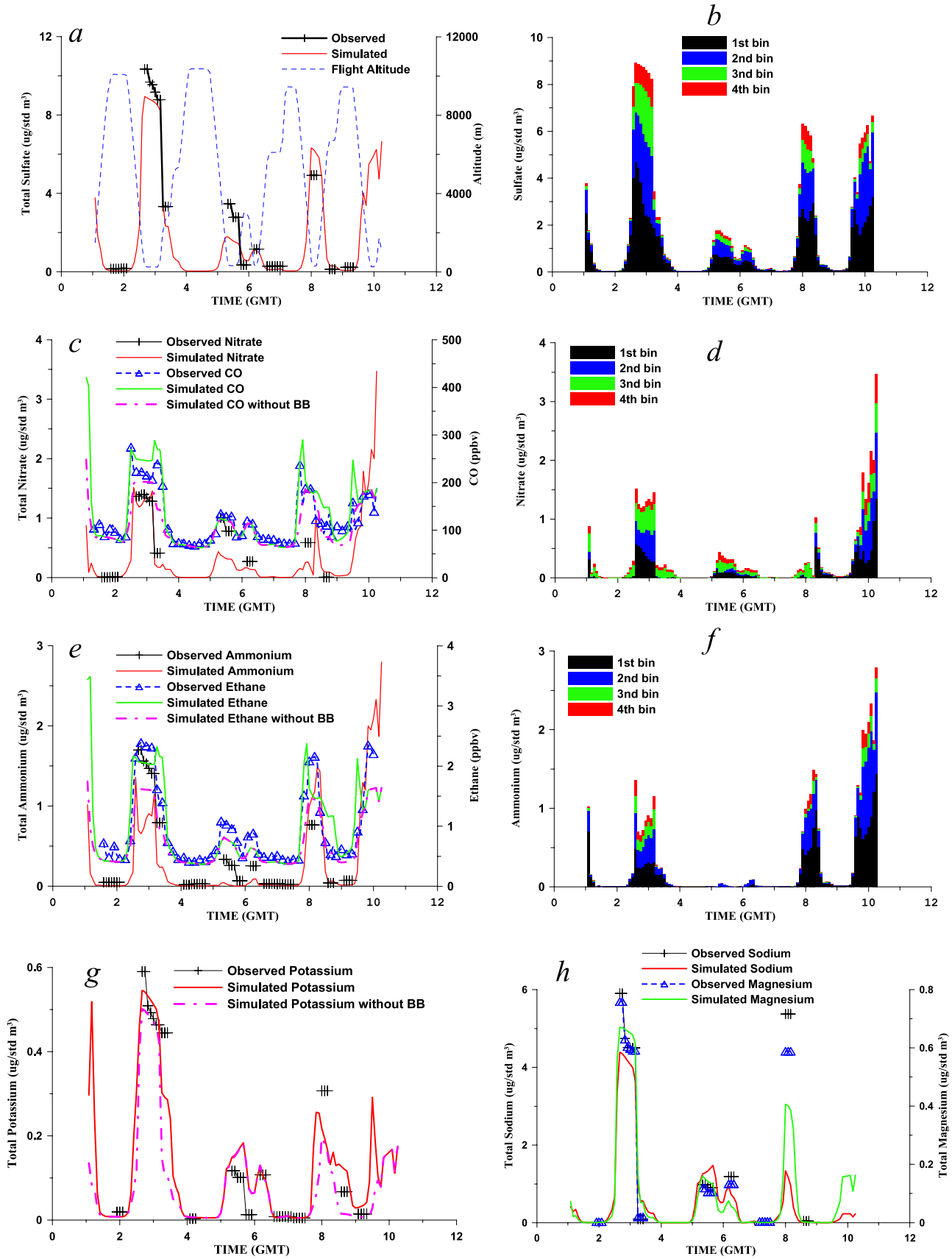
a
Observed
Simulated
Flight Altitude
Total Sulfate (ug/std m³)
Altitude (m)
TIME (GMT)
b
1st bin
2nd bin
3nd bin
4th bin
Sulfate (ug/std m³)
TIME (GMT)
c
Observed Nitrate
Simulated Nitrate
Observed CO
Simulated CO
Simulated CO without BB
Total Nitrate (ug/std m³)
CO (ppbv)
TIME (GMT)
d
1st bin
2nd bin
3nd bin
4th bin
Nitrate (ug/std m³)
TIME (GMT)
e
Observed Ammonium
Simulated Ammonium
Observed Ethane
Simulated Ethane
Simulated Ethane without BB
Total Ammonium (ug/std m³)
Ethane (ppbv)
TIME (GMT)
f
1st bin
2nd bin
3nd bin
4th bin
Ammonium (ug/std m³)
TIME (GMT)
g
Observed Potassium
Simulated Potassium
Simulated Potassium without BB
Total Potassium (ug/std m³)
TIME (GMT)
h
Observed Sodium
Simulated Sodium
Observed Magnesium
Simulated Magnesium
Total Sodium (ug/std m³)
Total Magnesium (ug/std m³)
TIME (GMT)

Figure 6

clearly seen in Figure 5d, with the increase in gaseous HNO_3 and the decrease in particulate nitrate from Julian day 63.5–64. The total aerosol nitrate and sulfate decreased during this period due to dilution and deposition.

[31] By Julian day 64 the air mass had moved to its farthest eastern location, where for the next 48 hours it moved slowly before being sampled by the DC-8. The aerosol nitrate oscillated over this period due to diurnal variations in temperature and relative humidity, important factors that influence the partitioning between the nitric acid and the aerosol. This partitioning of nitric acid is an important process. *Carmichael et al.* [2003a] summarized the performance of STEM-2K1 for TRACE-P mission, and showed that when these aerosol processes were ignored, gas-phase nitric acid was overestimated below 2 km. For this particular example associated with trajectory A, when we ignore the aerosol equilibrium process, the simulated HNO_3 concentration increased to the value equal to the sum of HNO_3 and particulate nitrate (i.e., ~1 ppbv) shown in Figure 5d. Without the aerosol interactions, HNO_3 was overestimated by a factor of 2 when compared to the DC-8 observations.

[32] After Julian day 65 (March 6), the air mass along trajectory A entered the marine boundary layer in the East China Sea, and mixed with sea salt, which resulted in a decrease in supermicron sulfate and nitrate. Sulfur oxides and nitric acid interacted with the sea salt and dust surfaces, and the particles grew in the high humidity conditions within the marine boundary layer. These processes are reflected in the changes in the fine fraction of nitrate and sulfate. The total aerosol nitrate and sulfate decreased during this period due to dilution and deposition.

3.1.2. DC-8 Flight 8 and P-3 Flights on March 7 and 9

[33] On March 9 the DC-8 and P-3 aircrafts performed flights 8 and 10, respectively, along 20°N (see Figures 2a–2i). Frontal activities brought a complex structure of different air mass origins along the flight paths [*Carmichael et al.*, 2003a]. In the middle altitudes (2–4 km), both aircraft encountered strong BB signals from Southeast Asia (see Figures 3c and 3d); in the low altitudes, air masses came mainly from northern China [*Tang et al.*, 2003b].

[34] Figure 6 shows the predicted and observed CO, ethane, sulfate, nitrate, ammonium, potassium, sodium, and magnesium along the path of DC-8 flight 8 (March 9). The situation is generally similar to that of DC-8 flight 7. The DC-8 flew through the postfrontal region into the prefrontal zone (4–6 GMT), and found high concentrations behind the front and fairly clean, well aged air ahead of the front. Behind the front sulfate concentrations were much higher than nitrate or ammonium, and sulfate was the main secondary-generated ion. This flight flew closer to the front (nearly along 20°N) for longer periods than the previous flight that flew more perpendicularly to the front. When flight segments close to the front are compared (4–5 GMT DC-8 flight 7 and 2–4, 8–9, and 9–10 GMT DC-8 flight 8) the aerosol distributions are found to be very similar. This flight did observe appreciable amounts of potassium due to the biomass burning and biofuel combustion. Figure 6g shows that the simulation without BB emissions underestimated potassium in some flight segments. Figures 6c and 6e show a similar pattern for CO and ethane. These results suggest that our estimates of potassium (as well as CO) emissions from biomass burning may be underestimated. To further explore the impact of biomass potassium on the aerosol composition, simulations were preformed using burning-source potassium emissions increased by a factor of 5. Under these conditions, submicron nitrate in BB impacted segments increased by at most 30% and ammonium decreased by at most 12%. No other influences to other aerosol constituents were found.

[35] On March 7 and 9 the P-3 aircraft performed its ninth and tenth flights, and these flight paths partially overlapped with the DC-8 flights on the same days (Figures 2a–2i). The P-3 aircraft flew mainly below 6 km. The PILS instrument measured aerosol ions in particles of diameter $\leq$1.3 μm. Figure 7 shows the simulated submicron sulfate (sum of the first and second bins) compared to the P-3 measurements. For both flights most of the sulfate was in the submicron particles. In these two flights the calculated mean sulfate fine ratio was ~0.9. The sulfate size distribution on these P-3 and DC-8 flights reflect sulfate formation in polluted air masses not heavily influenced by dust.

[36] P-3 flight 9 encountered a relatively fresh megacity plume from 6 to 7 GMT. Trajectory B (Figure 4c) indicates that this air mass passed nearby Shanghai one day before it arrived at the P-3 flight at 6:55 GMT, and traveled at a low altitude (<1.5 km). The simulated aerosol composition of this urban plume over the city and at the time it was sampled by the P-3 is shown in Figure 8, along with the observed composition. Figures 8a and 8b show that over the source area nitrate represented more than 25% of the soluble submicron mass, and more than 50% of the supermicron mass of all secondary ions, while sulfate was concentrated in the submicron mode. When this air mass reached the aircraft, its composition changed in a manner similar to that discussed before for trajectory A. As SO_2 was oxidized to sulfate, the sulfate mass increased in all size bins, and nitrate was displaced from the aerosol phase, first from the submicron particles, and then from the supermicron particles. When this air mass arrived at the P-3 flight path, nitrate accounted for about 17% of the submicron secondary ions, and ~26% of the supermicron mass. The PILS measurements indicated that the nitrate mass percentage was ~14%. Along this trajectory the predicted ammonium abundance remained at ~19%. These results illustrate that sulfate displaces nitrate under cation-limited condition as the megacity plume moves out over the sea.

3.2. Dust Events

[37] Dust storms are frequent during the springtime in east Asia. Both TRACE-P and ACE-Asia flights encountered dust events. The greatest dust storm during the

Figure 6. Observed and simulated (a) total sulfate, (c) nitrate and CO, (e) ammonium and ethane, (g) potassium, (h) sodium and magnesium, and simulated ion size distributions of (b) sulfate, (d) nitrate, and (f) ammonium, along the path of DC-8 flight 8, March 9, 2001. Simulated CO, ethane, and total potassium without biomass burning emissions are presented in Figures 6c, 6e, and 6g (pink dashed line).

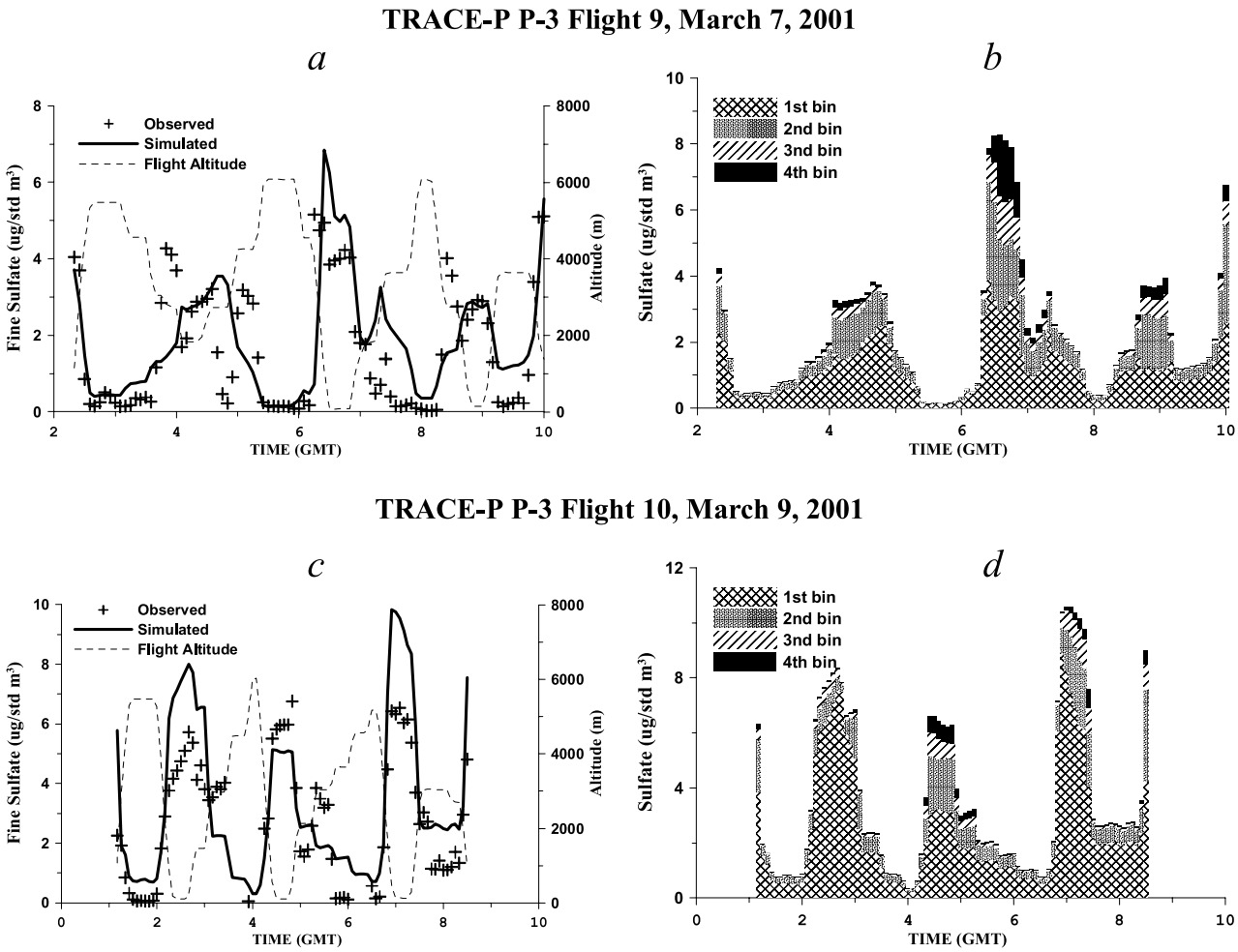

Figure 7. Observed and simulated fine sulfates and sulfate size distribution along P-3 flight 9 (March 7) and 10 (March 9).

campaign occurred from April 4 to 14. *Tang et al.* [2004a] described this dust event and corresponding simulations that were compared to satellite images, surface weather stations, and C-130 measurements. That paper discussed the impact of heterogeneous reactions involving dust on gaseous species, with special focus on C-130 flight 6 that recorded the strongest dust encounter. Windblown dust affects aerosol composition and distribution, since dust is rich in calcium, magnesium, and carbonates. These ions and their size distributions influence the uptake of secondary species, through both heterogeneous reactions and equilibrium processes. The impact of dust on the aerosol ion composition is discussed in this section.

3.2.1. Regional Evolution

[38] Figure 9 shows the total dust (line contours), the dust fresh ratio (weighted average of all size bins) (colored) defined in equation (1), and sulfate concentration and coarse ratio (the mass of the supermicron particles divided by the total mass) over the period April 7–13, as the great dust storm traveled across east Asia and was observed by the C-130 and Twin Otter aircrafts, and ship *Ronald Brown.* *Tang et al.* [2004a] described the dust simulations in detail. This great dust storm arose in northwestern China-western Mongolia in association with a cold air outbreak. On April 7 the dust storm reached eastern Mongolia/northeastern China, where new dust emissions were generated by the strong surface winds that accompanied the cold front. The model-predicted dust fresh ratio measures the extent to which the dust has been aged by chemical processing. Strong gradients are shown, with well-aged aerosol (low values) found along the leading edge of the dust front, and ratios increasing with distance behind the front. At the storm center, the dust fresh ratio approached 0.95, and the sulfate coarse ratio was 0.6. As this dust storm traveled to the east, anthropogenic pollutants from east Asia were transported to the north toward the center of the low-pressure system. This polluted air mass was transported ahead of the front in middle altitudes, as the storm moved out over the Japan Sea. As discussed by *Seinfeld et al.* [2004] and *Tang et al.* [2004a], the bulk of the dust in this storm was concentrated at altitudes between 2.5 and 6 km. C-130 flight 5 (not presented) flew over the Japan Sea on April 8 and observed this stratified distribution of dust and coarse anions above 2.5 km, and fine-mode secondary pollution aerosol (sulfates and nitrates) below.

[39] On April 9 the second branch of this dust storm approached Beijing. The cold front at this time extended from the northeast to southwest, and high-concentrations of

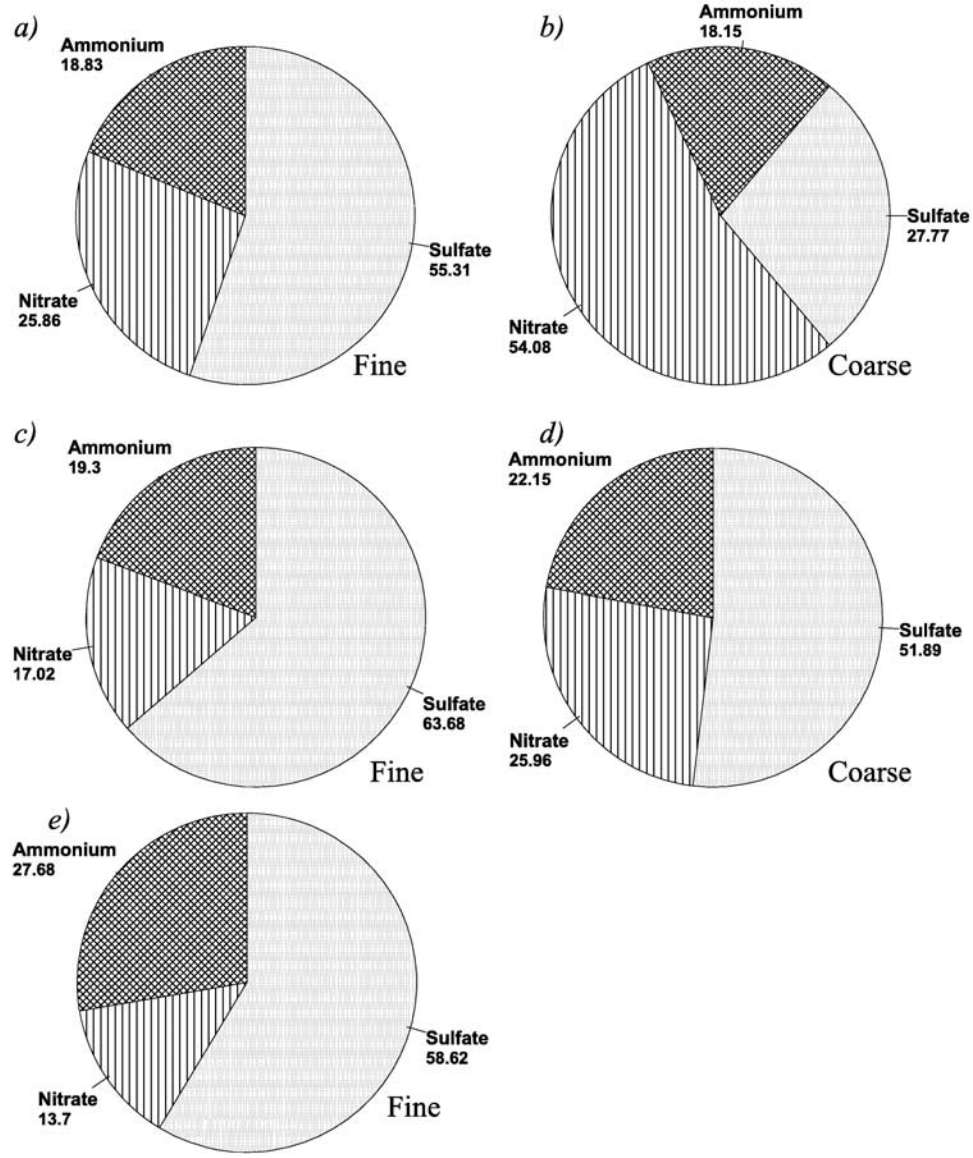

Figure 8. Mass percentages of submicron and supermicron secondary ions when the trajectory C (a, b) passed nearby Shanghai, (c, d) arrived at P-3 flight 9 at 6:55 GMT, and (e) PILS observation at 6:55 GMT.

sulfate (>20 $\mu g/m^3$) were distributed along the front. At this time the sulfate concentration distribution was similar to that on April 7, but the coarse ratios were different. On April 7 the simulated dust loading near Beijing was <1000 $\mu g/m^3$ and by April 9 had increased to over 2000 $\mu g/m^3$. The regions with high sulfate coarse ratios (>0.5)) were distributed along the front. When the dust front mixed with fresh pollutants, the aerosol aged quickly, represented by the air masses with dust fresh ratios <0.1. On April 11 the dust storm continued moving to the southeast and extended as far south as Hong Kong, and the major outflow (which was confined to altitudes below ~3 km) was positioned over the Yellow Sea. The dust over the east coast of China had its fresh ratio reduced to less than 0.4. In heavy-polluted areas like Beijing and Qingdao the dust fresh ratio was less than 0.2. The sulfate coarse ratio was about 0.3 over the Yellow Sea. On April 13, the low level winds over southeast China shifted to the southwest, and the dusty air mixed with pollutants from southern China was transported into the Yellow Sea. This air mass was well aged, with fresh ratios less than 0.1.

[40] The predicted sulfate coarse ratios show clearly the interactions between dust and pollutants. The dust and pollution distributions were segregated on April 7–9 as shown by the low sulfate-coarse fractions in the high sulfate loading areas. In this polluted region, fine mode sulfate dominated. The high coarse fractions that surround this patch reflect sulfate associated with dust and sea salt. On April 11 and 13, the dust and pollution were well mixed and the sulfate coarse fraction increased due to sulfate formation on the dust particles. Further details are discussed below in relation to the aircraft observations.

3.2.2. C-130 Flight 6

[41] Figures 10a–10k shows simulated and observed submicron and total aerosol ion concentrations along C-130 flight 6 on April 11, whose path is shown in

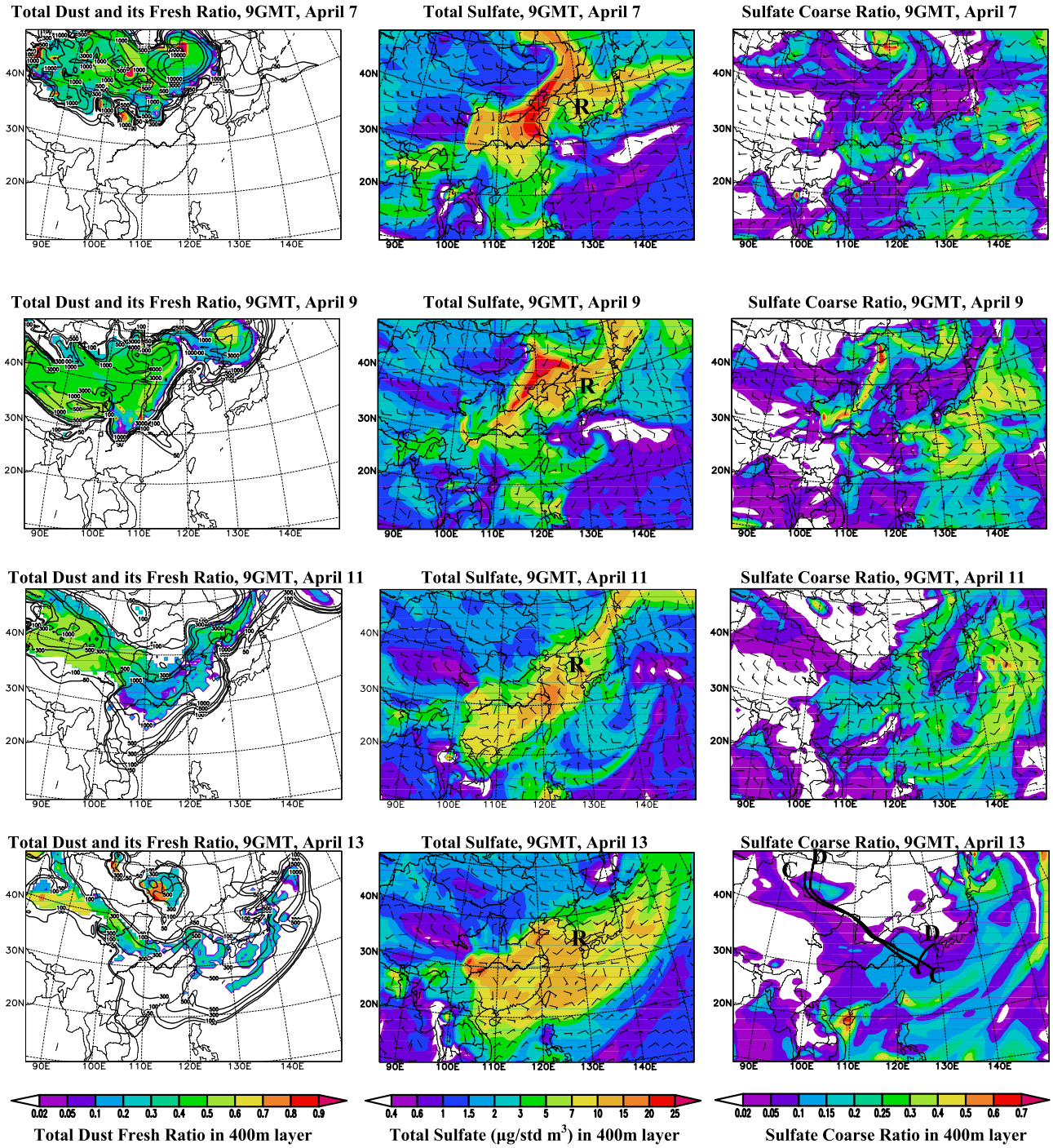

Figure 9. Simulated (left) total dust and its fresh ratios, (middle) total sulfate, and (right) sulfate coarse ratios in model's 400 m layer on April 7, 9, 11, and 13. Total dust is presented in the left panels with black contour lines in $\mu g/m^3$ (standard state). Trajectories C (arrived at the path of C-130 flight 8 at 7:08 GMT) and D (arrived at RB in 500 m level at 0 GMT, April 14) are shown in the bottom right plot (sulfate coarse ratio on April 13). Locations of ship *Ron-Brown* are marked with "R" in middle-column panels at corresponding times.

Figures 2a–2i. C-130 flight 6 flew at low altitudes (<400 m) over the Yellow Sea, where it sampled dust mixed with pollution outflow. The submicron ions were measured by the PILS instrument [*Lee et al.*, 2003] with a sampling frequency of ~3 min. The total ion concentrations were measured by the TAS instrument [*Kline et al.*, 2004], with a sampling time of ~30 min. The simulations with and without dust show significant differences in the calculated ions. Calcium and magnesium are the main primary ions associated with dust. The predictions of submicron calcium and fine-mode magnesium with dust for the outbound leg (2–3 GMT) are within a factor of 2 of the observed, which

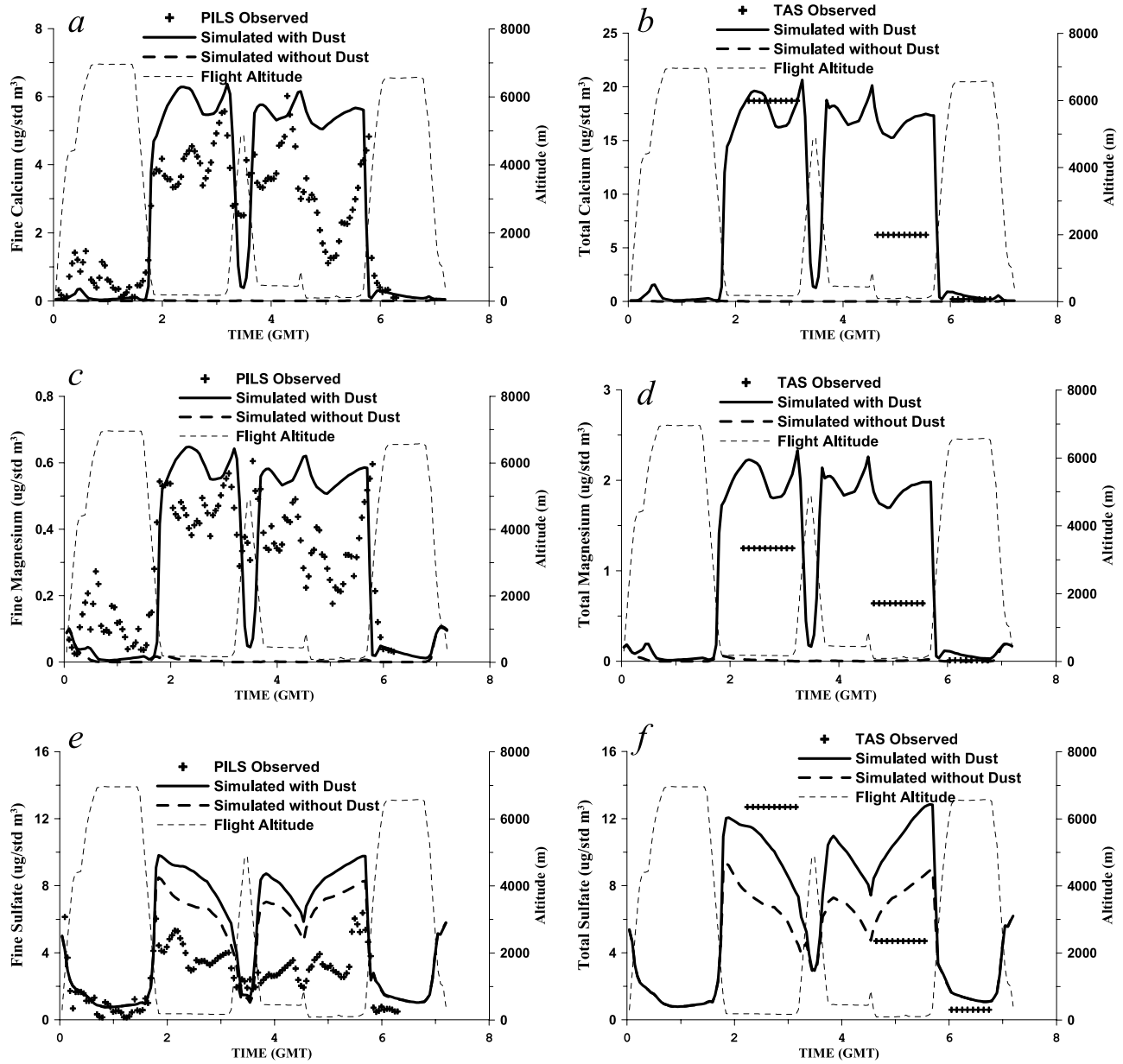

Figure 10. Observed and simulated (with and without dust) (a) fine Ca, (b) total Ca, (c) fine Mg, (d) total Mg, (e) fine sulfate, (f) total sulfate, (g) fine nitrate, (h) total nitrate, (i) fine ammonium, (j) total ammonium, and (k) simulated total Ca in $CaSO_4$ and $Ca(NO_3)_2$ along the path of C-130 flight 6.

may be fortuitous considering the large uncertainties associated with predictions of dust mass emissions [cf. *Huebert et al.*, 2003]. The predictions did not capture the decrease in the aerosol ions on the return leg. As shown in Figure 9, the pollution front was quite narrow as it moved across the Yellow Sea on April 11, and the timing of the passage was a few hours later in the model than that observed. The observations and predictions indicate that an appreciable portion of the dust occupied the fine mode (20–30% by mass as indicated from the calcium values (Figures 10a and 10b)). Sodium concentrations were also enhanced during the dust events. The simulation without dust missed these ion signals.

[42] Freshly emitted Asian dust is alkaline, with calcium mainly in the form of $CaCO_3$. Dust can affect secondary aerosol concentration through equilibrium and heterogeneous reactions. Both processes lead to the enhancement of particulate nitrate and sulfate. Figure 10f shows that the predictions with dust agree better with the observations for total sulfate, and that the simulation without dust underestimated total sulfate for the outbound flight leg over the Yellow Sea. However, submicron sulfate was overestimated. The observations and the predictions indicate that the supermicron fraction of total sulfate was ~0.7 on the outbound leg, and 0.1 on the inbound leg.

[43] Under conditions of this flight the gas-aerosol equilibrium of nitrate is determined mainly by the distributions of calcium and gaseous ammonia. Figures 10g and 10h show that the predictions with dust better represent the observed nitrate concentrations, and that the nitrate size

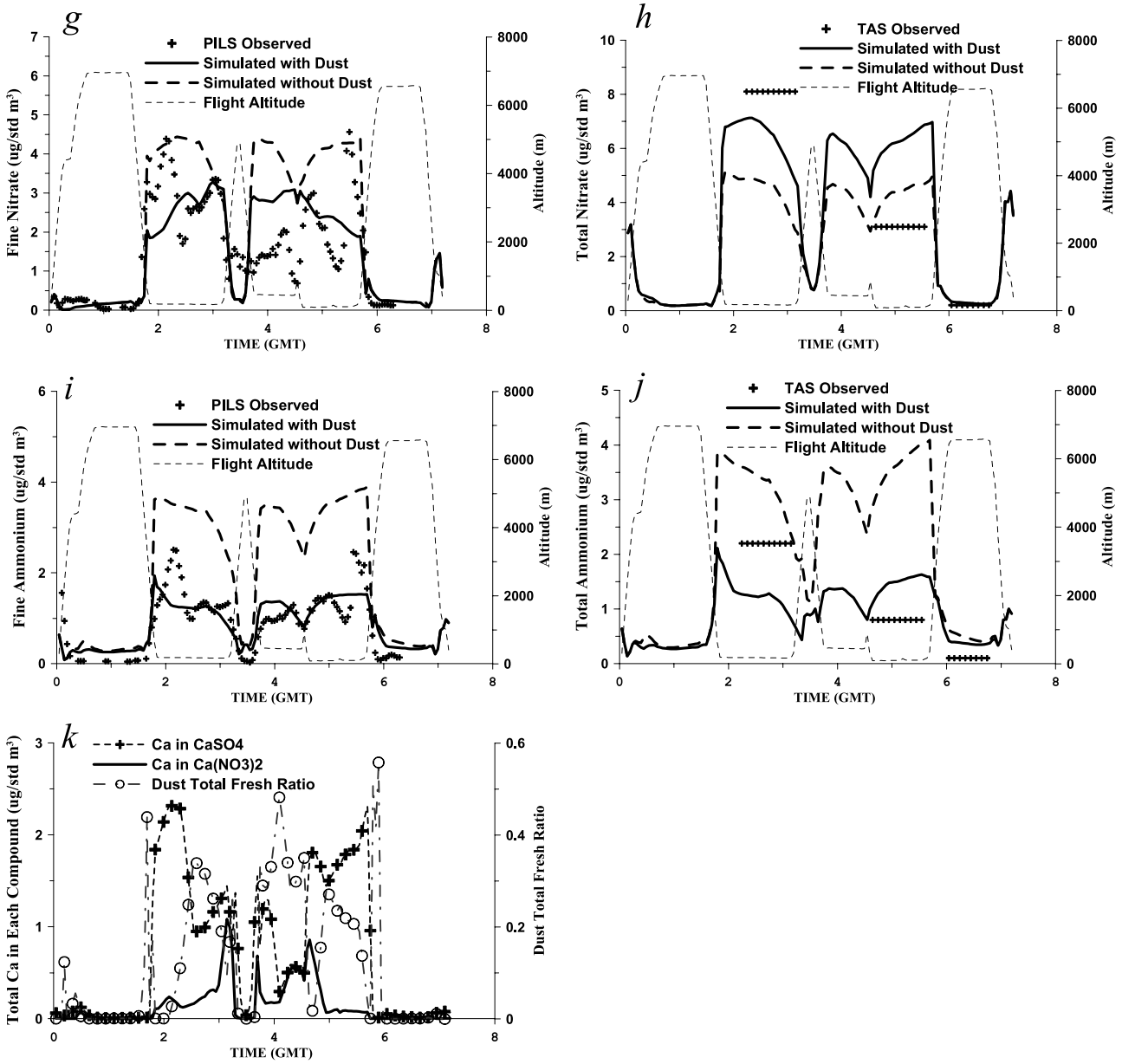

Figure 10. (continued)

distribution is similar to that of calcium, shown by both model and observations to be ~70% in the supermicron fraction. Owing to the large amounts of calcium and NH_3 in the outflow, the aerosol remains alkaline, and most nitrates were partitioned into the aerosol (and calculated HNO_3 concentrations were very low (not measured on the C-130)). Dust also significantly impacts ammonium. Figures 10i and 10j show that the simulation without dust significantly overestimated ammonium, and that the simulation with dust agrees well with the measurements. The presence of dust is found to reduce the ammonium in the aerosol by 50%. Both the model and observation indicate that ammonium was restricted to the submicron mode.

[44] Carbonate is released from the aerosol in the form of CO_2 as strong acidic ions such as SO_4^{2-} and NO_3^- react with the dust calcium. The amount of carbonate in the aerosol thus provides an indication of the chemical age of the particles. The fresh dust ratio discussed previously is a measure of this age. The calculated dust fresh ratio of the total aerosol is shown in Figure 10k. Also shown are the salt forms of calcium calculated by SCAPE. These results indicate that the nitrate and sulfate in the outflow is a mixture of calcium, magnesium and sodium salts, and ammonium sulfate and nitrate. When the dust loading reached its maximum value around 2 GMT (Figure 10b), $CaSO_4$ also reached its peak value of 2.4 $\mu g/m^3$ (in standard state), and calcium nitrate was ~0.2 $\mu g/m^3$ (in standard state). The dust was well aged as represented by the low dust total fresh ratio. During the period from 2 to 3 GMT, high-concentration and relatively fresh dust was mixed into the air mass, and calcium nitrate levels increased as calcium sulfate decreased. The largest fresh ratios were found at high altitudes.

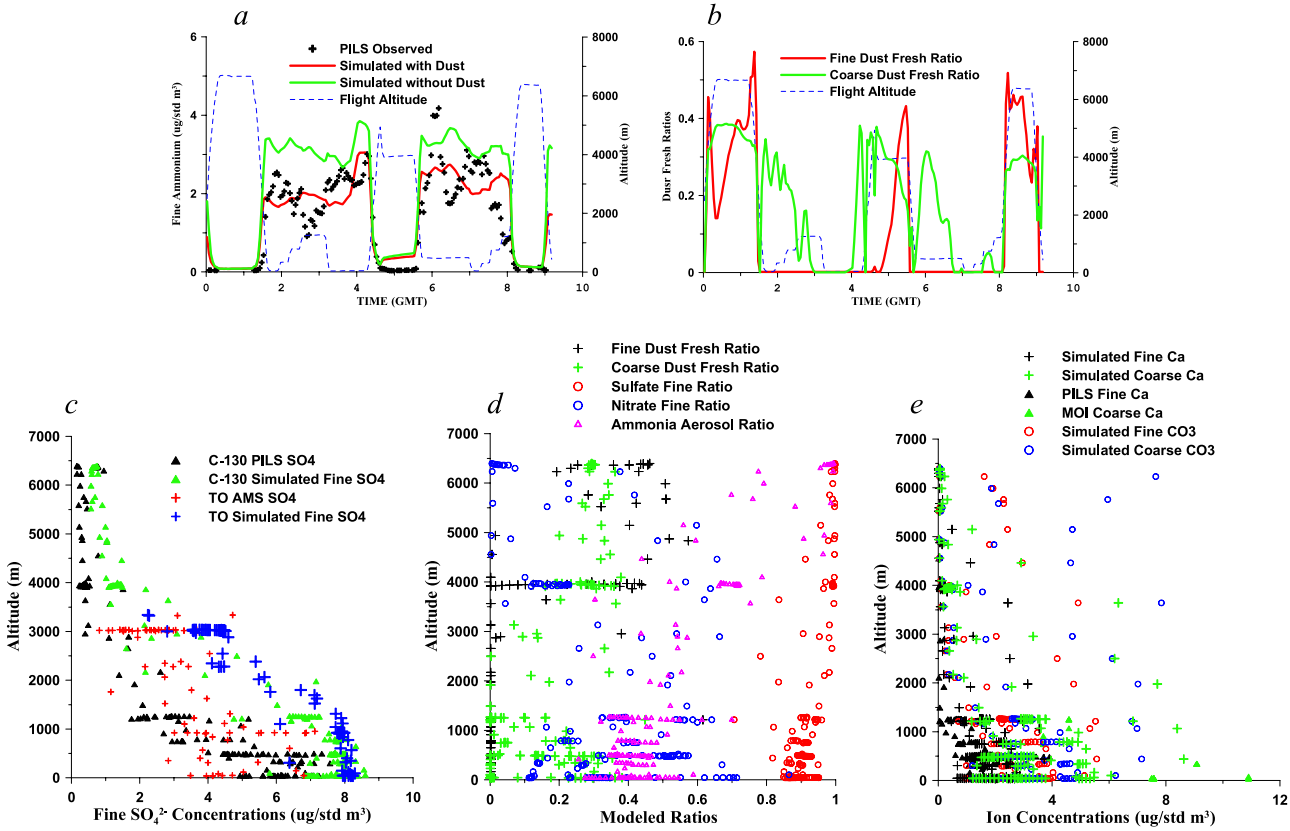

Figure 11. C-130 flight 7 results: (a) simulated and observed fine ammonium along this flight path; (b) simulated dust fresh ratios along this flight path; (c) observed and simulated fine sulfate profiles in C-130 flight 7 and Twin-Otter flight 8; (d) dust fresh ratios, sulfate and nitrate fine ratios, and ammonia aerosol ratio in vertical profile; (e) calcium and carbonate vertical distributions.

3.2.3. April 12 and 13

[45] This dust storm was sampled again over the next few days, by the C-130 flight 7 (April 12) and 8 (April 13), and the Twin-Otter flight 8 (April 12) and 9 (April 13). The C-130 flight 7 flew nearly the same flight path as C-130 flight 6 (Figures 2a–2i). However, the outflow into the Yellow Sea had different characteristics on flight 7 than those observed during flight 6. As shown in Figure 9, during the C-130 flight 7 the outflow into the Yellow Sea came from the northwest and contained large amounts of dust as well as pollutants from the Beijing-Tianjin corridor. By April 12 the flow had shifted to westerly winds and the dust levels decreased (Ca^{2+} lower by factor of 3), while the pollution levels (e.g., SO_2, NO_x, SO_4^{2-}, NO_3^-, NH_4^+, K^+) over the Yellow Sea increased by a factor of 2 compared to the day before. The dust was also more chemically aged.

[46] Figure 11a shows the measured and simulated submicron ammonium in the presence and absence of dust along this flight. The simulation without dust overestimates submicron ammonium, though the overestimation was not as great as that for C-130 flight 6. On April 12, both C-130 flight 7 and Twin-Otter (TO) flight 8 (Figures 2a–2i) encountered aged dust mixed with pollutants. Figure 11c shows the measured and simulated submicron sulfate profiles for these two flights whose flight paths partially overlapped. Both observation sets show that the outflow was confined to altitudes below 3 km in the postfrontal region, and that within the marine boundary layer the ion values showed substantial variability (sulfate values varied from 2 to 7 $\mu g/m^3$). The simulated profiles along the C-130 and TO flight paths also exhibit the same general features, with a tendency to overestimate sulfate by ~20% at the altitudes below 1 km. The model shows significantly less variability than the observations, implying that an increase in the spatial resolution of the model may be necessary to capture more of the observed variability.

[47] The low-altitude dust aged faster than the high-altitude dust as a result of the high pollutant loading, including NO_x, HNO_3, SO_2, SO_4^{2-}, NO_3^- etc. Figures 11b and 11d show that the fine dust fresh ratio was nearly 0 at the low altitudes, indicating that the fine dust surface was saturated, with calcium in the fine dust surface in the forms of $CaSO_4$ and $Ca(NO_3)_2$. The aged dust was found to have no influence on submicron sulfate (not shown). Above 4 km the dust was relatively fresh (Figure 11d), and dust and pollutant loadings were low. Sulfate at these altitudes was concentrated in the submicron fraction in the form of $(NH_4)_2SO_4$, and nitrate was partitioned into the supermicron fraction. Predicted calcium is shown in Figure 11e. Both the observations and the predictions show that calcium in the lowest 2 km range from 1 to 12 $\mu g/m^3$ (in standard state). The calculated carbonate concentrations reflect the alkaline-acidity balance. Usually the supermicron aerosol was predicted to be more alkaline than the fine-mode particles. The

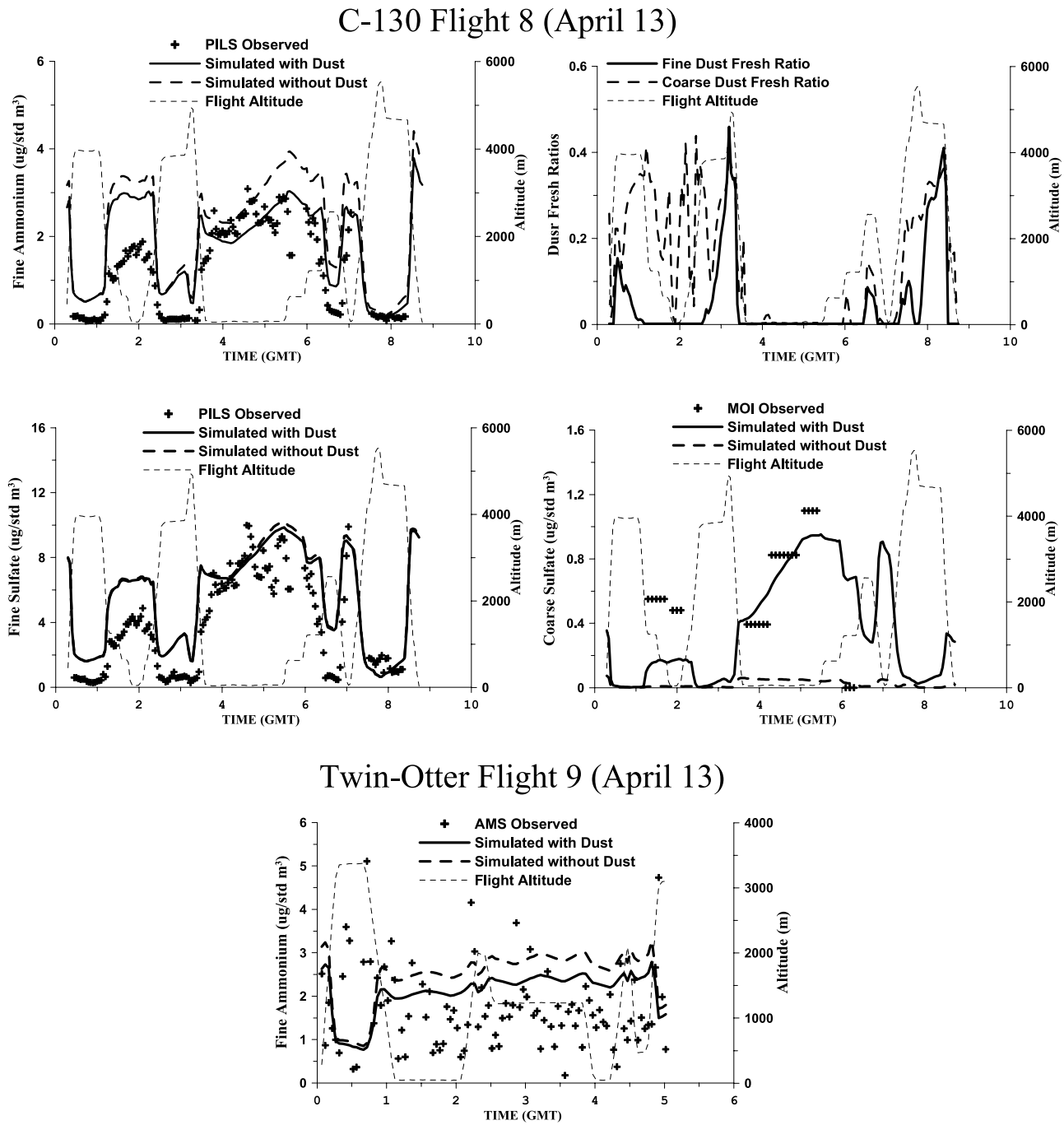

Figure 12. Simulated and observed (top left) fine ammonium, (top right) dust fresh ratio, (middle left) fine sulfate, (middle right) coarse sulfate along the C-130 flight 8, and (bottom) simulated and observed fine ammonium along the Twin-Otter flight 9.

calculated carbonate concentrations show a broad minimum between the altitudes of 3–4 km. Below this altitude, high dust loading and alkaline sea salt benefited the CO_2 uptake. Above this altitude the relatively high dust fresh ratio led to increased carbonate concentration.

[48] On April 13 the C-130 flight 8 and Twin-Otter flight 9 were carried out in a region south of Japan (Figures 2a–2i) and sampled the aged and diluted dust air mass. Figure 12 shows the measured and predicted submicron ammonium with and without dust along these two flights. This situation is similar to that in C-130 flight 7. For the same low-latitude flight segments the coarse dust fresh ratio was higher than that for the fine mode, and much lower than that during C-130 flight 6 (Figure 10k). Our simulations show that the submicron dust ages faster than the supermicron dust because the former has a larger surface area per unit dust mass. Figure 12 shows the simulated and observed submicron and supermicron sulfate along the C-130 flight 8 track. Dust did not influence the submicron sulfate, but significantly increased the supermicron sulfate concentra-

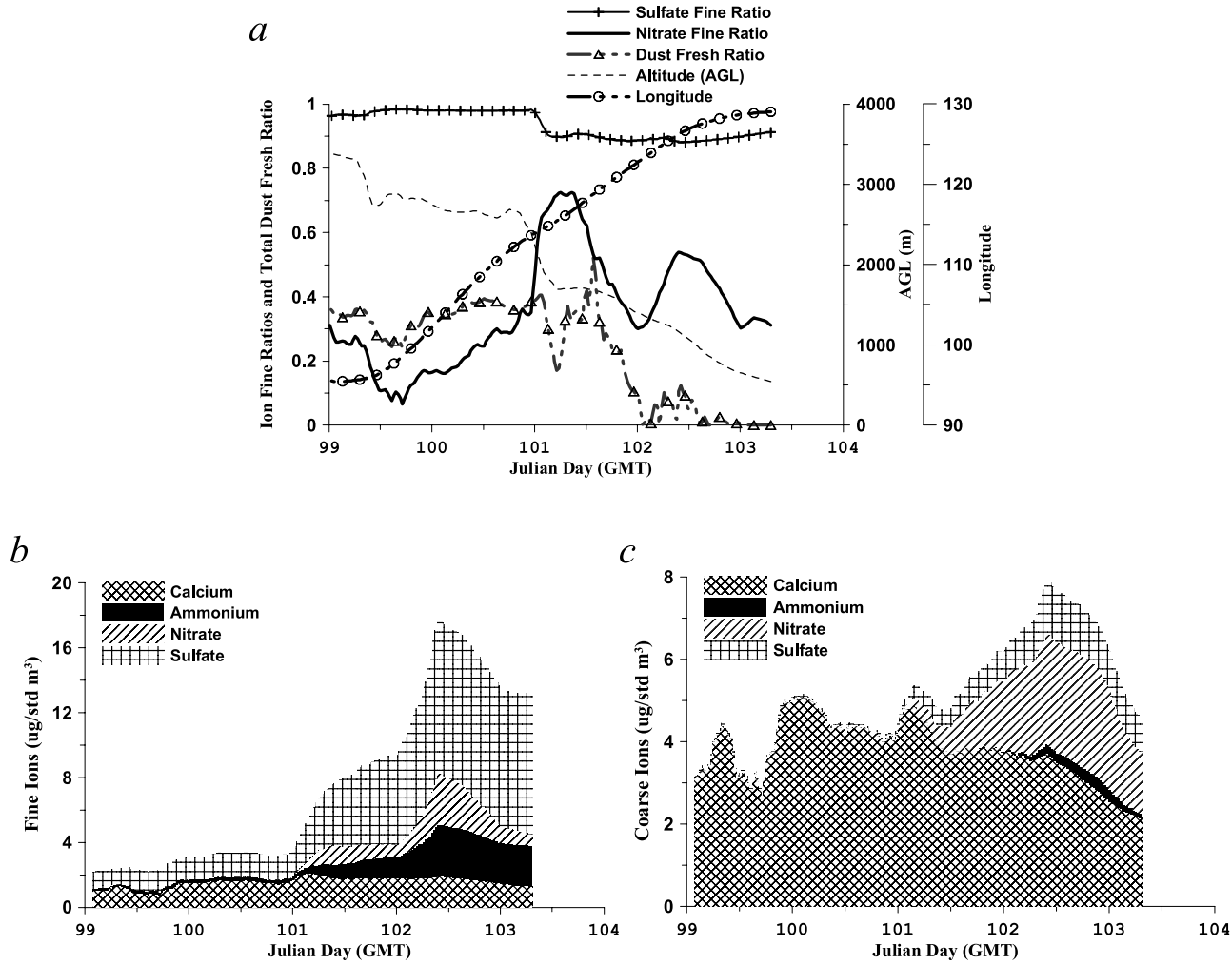

Figure 13. Simulated (a) sulfate and nitrate fine ratios and dust fresh ratio, (b) fine aerosol compositions, and (c) coarse dust compositions along trajectory D of Figures 10a–10k, which arrived at the path of C-130 flight 8 at 7:08 GMT.

tion. Nevertheless, most of the sulfate in this air mass was in the submicron fraction.

[49] Figure 13 shows the aerosol variations along trajectory C (Figure 9) that arrived at the C-130 flight 8 track at 7:08 GMT. On Julian day 99 (April 9) the air mass was 3.5 km over western Mongolia, where it had a high dust loading, with 80% of the aerosol mass in the coarse mode. The air mass had elevated sulfate, but little nitrate. The trajectory descended as it moved to the southeast. When this trajectory entered the polluted continental boundary layer over eastern China on April 11 (Julian day 101), it encountered anthropogenic pollutants, and sulfate and nitrate levels increased. The sulfate fine ratio decreased, while the dust fresh ratio decreased to lower than 0.2, and then increased when fresh dust was mixed into the air mass. During the period Julian day 101–102.5 the pollution interacted with the dust, and fine and coarse mode nitrate and sulfate increased. Sulfate and ammonium were largely in the submicron fraction, with nitrate largely in the supermicron particles. When this trajectory reached the coastal polluted areas (around 120°E in longitude) on Julian day 102 and its height decreased to below 1.5 km, dust quickly became saturated, and the decrease in the nitrate fine ratio paralleled the decline of the dust fresh ratio. After the dust lost its activity, the sulfate fine ratio leveled off. The supermicron concentrations decreased as the large particles were lost by deposition. This trajectory shows that the dust aging is strongly associated with the encounter with pollutants.

3.3. Events Near Marine Surface

[50] The NOAA research vessel *Ronald H. Brown* sampled marine boundary layer air in the Japan Sea, East China Sea, and western Pacific Ocean from March to April. Shipboard measurements included characterization of chemical composition of the submicron and supermicron particles. The details of the observed values over the period Julian day 94–05, during which the ship encountered the prefrontal and postfrontal conditions of the large dust storm, are discussed by *Bates et al.* [2004]. The ship cruise track is shown in Figures 2a–2i, and its locations on specific days are shown in Figure 9. Observed and simulated values of ozone, CO, and total aerosol Na^+ are presented in Figure 14. On Julian day 90 the ship was south of Tokyo, and by Julian day 97 it had traveled around the western tip of Japan and

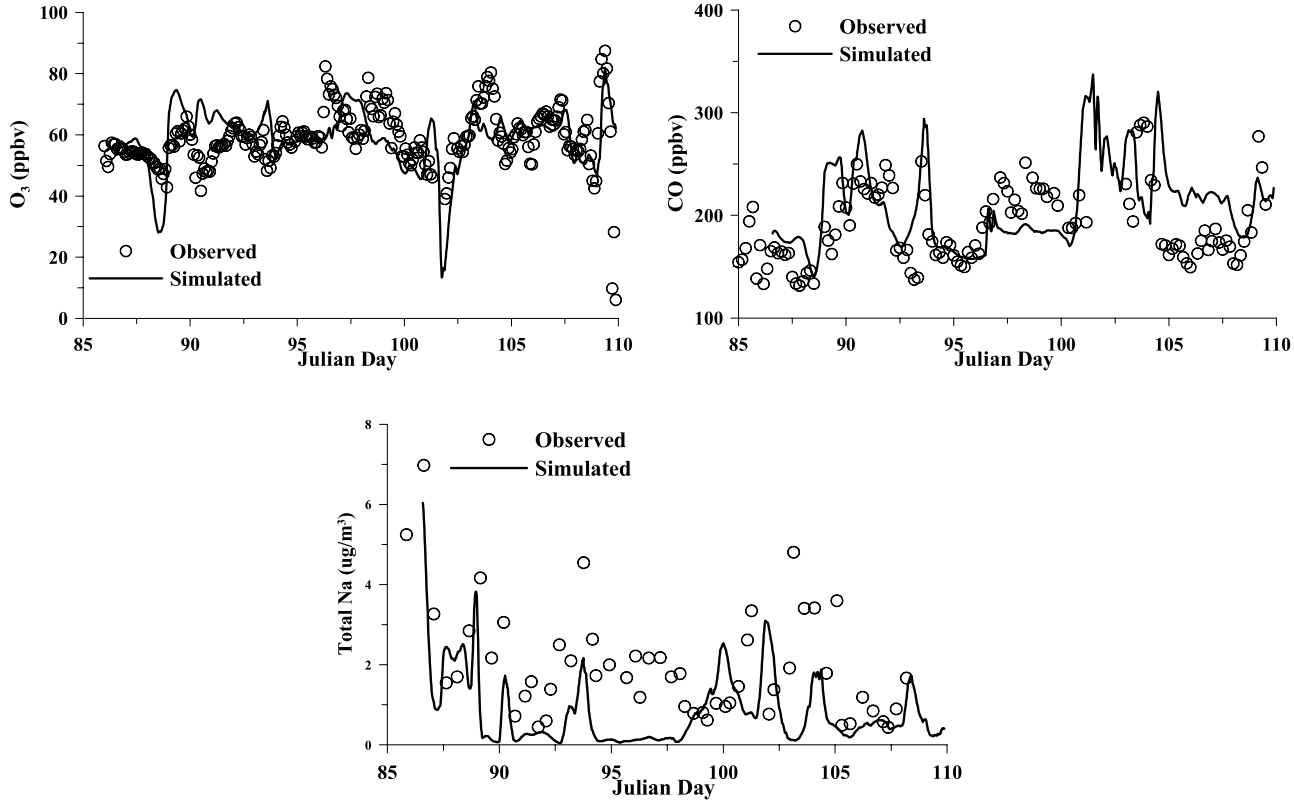

Figure 14. Simulated and observed O_3, CO, and total sodium concentration along the cruise path of the R/V *Ronald Brown*. The aerosol ion was measured with two-stage multijet cascade impactor [*Quinn et al.*, 2000].

arrived in the Japan Sea, where it remained until Julian day 103. While in the Japan Sea the ship sampled the outflow associated with the large dust storm discussed previously and illustrated in Figure 12. In the Japan Sea the marine boundary layer was enhanced in pollutants, with ozone levels greater than 60 ppbv and CO exceeding 200 ppbv. During the great dust event from April 4 to 14, a cold front entrained the dust and anthropogenic pollutants to the east and formed the Asian outflow. As the dust front passed over the Japan Sea, the pollution levels increased dramatically, with CO reaching a maximum of >300 ppbv. Dust heterogeneous reactions contributed to the simultaneous low concentration of O_3, as shown in Figure 14, and discussed by *Tang et al.* [2004a]. Since the ship sampled near the sea surface, sea-salt sodium was usually enhanced (between 2 and 4 $\mu g/m^3$), and sea salt contributed to the elevated sulfate concentrations.

[51] Observed and simulated submicron and supermicron aerosol compositions over the period of Julian day 94–105 on the ship are shown in Figure 15. The arrival of the polluted air just preceding the dust front on Julian day 100 is indicated by the large increase in the submicron sulfate. This air mass was also heavily impacted by emissions from the Miyaka-jima volcano plume as indicated by trajectory analysis (not shown), and by the high levels of SO_2 (as discussed by *Bates et al.* [2004]). The submicron aerosol consisted of sulfate and ammonium. The model also predicted submicron nitrate, but this was not observed. On Julian day 101 the dust-rich air mass was subsiding and mixed with the polluted air mass; this is clearly seen in the increase in the supermicron calcium, sulfate, and nitrate. Both the observations and the model show that nitrate was dominantly partitioned into the supermicron fraction, while sulfate was largely in the submicron mode, but with a nonnegligible supermicron fraction. From the observed Al concentrations the supermicron fraction of dust varied from 90% to a minimum of ~70%, while the supermicron fractions of non-sea-salt (nss) sulfate and nitrate reached maximum values of ~20% and >90%, respectively. During Julian days 101–105 the ship sampled the postfrontal outflow, with dust mixed with fresh pollutants. Trajectory D for Julian day 104 (Figure 9) indicates that the air mass observed was heavily influenced by Shanghai emissions; this air mass was enhanced in submicron and supermicron sulfate and nitrate. In this air mass, submicron nitrate was both predicted and observed, with characteristics similar to those discussed in relation to Figure 13.

[52] Sea salt also plays an important role in influencing the size and chemical composition of the inorganic ions in the Asian outflow. An important feature observed and predicted is the deficiency in aerosol Cl^- as the result of the interaction between the secondary acidic ions and sea salt. This is clearly evident in the filter and single particle measurements, and the model predictions. The single particle measurements with Aerosol Time-of-Flight Mass Spectrometry (ATOFMS) [e.g., *Prather et al.*, 1994; *Gard et al.*, 1997; *Guazzotti et al.*, 2003] and the model results (calculated as the difference between simulations with and without aerosol interactions) are shown in Figure 15e. The presence of sulfate (m/z 165 corresponding to $Na_3SO_4^+$), nitrate (m/z

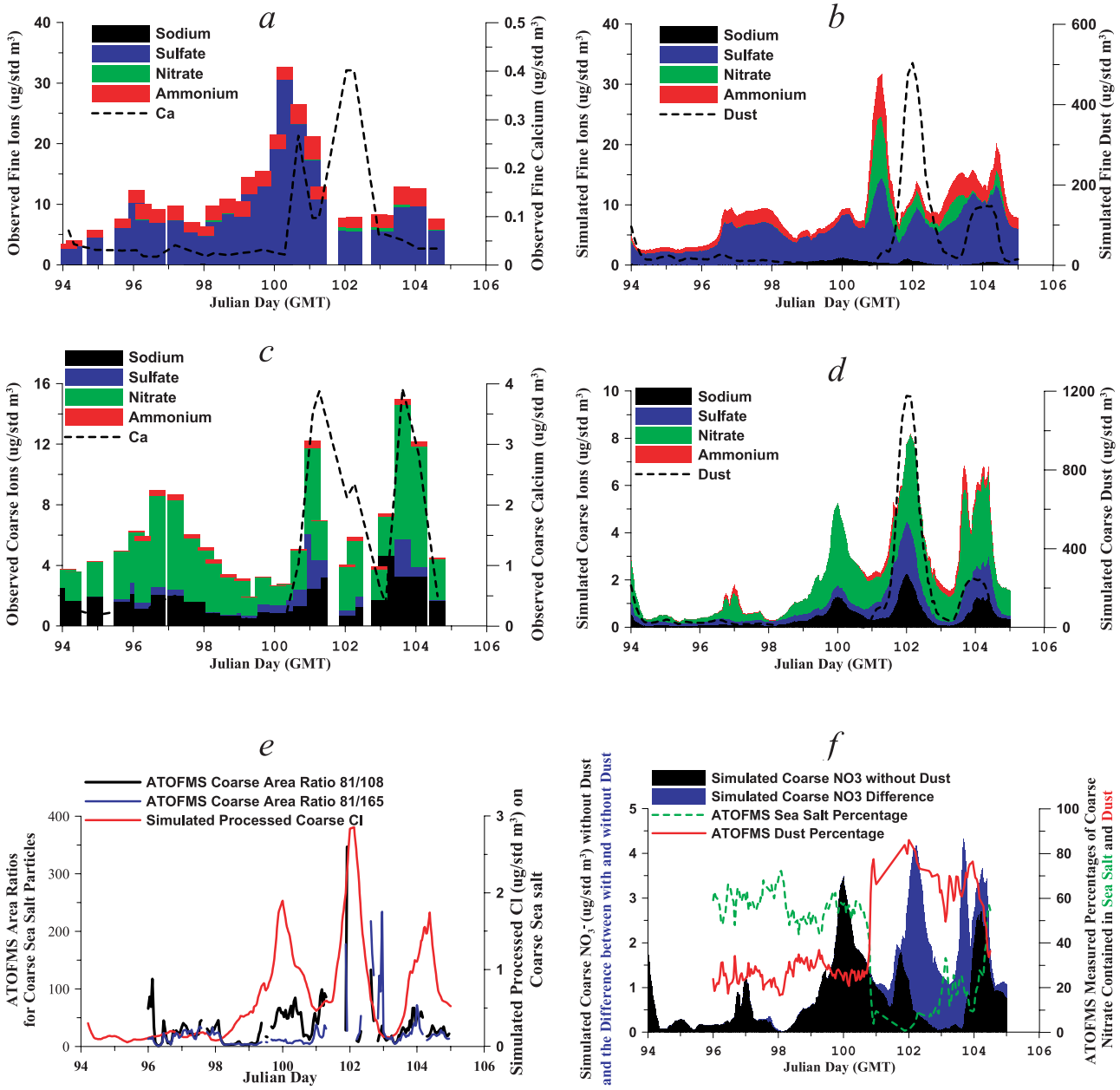

Figure 15. (a) Observed fine ions, (b) simulated fine ions, (c) observed coarse ions, (d) simulated coarse ions, (e) ATOFMS measurements compared to simulated processed coarse sea salt, and (f) simulated nitrate difference due to dust along the cruise path of R/V *Ronald Brown* from April 4 to 16.

108 corresponding to $Na_2NO_3^+$) in the ATOFMS supermicron sea-salt particles indicate chemical processed sea salt. Area ratios for the different ions present in the ATOFMS mass spectra of supermicron sea salt particles representing the presence of sulfate (m/z 165, $(Na_3SO_4)^+$), nitrate (m/z 108, $(Na_2NO_3)^+$), and chlorine (m/z 81, $(Na_2Cl)^+$; indicative of how reacted/unreacted a sea salt particle is) are presented with 1-hour resolution. The temporal evolution for the 81/108 and 81/165 area ratios highlight the relative changes in the amount of nitrate or sulfate present in sea salt particles. The predictions simulated processed chloride (equivalent to the amount of Cl^- liberated from sea salt due to interaction with sulfate and nitrate and calculated as the difference between simulations with and without aerosol interactions) on coarse sea salt (Figure 15e) shows the same trends as that measured, with highly processed sea salt events associated with: the arrival of the pollution front (~Julian day 100); the heavy dust period (Julian day 102); and the postfrontal outflow downwind of Shanghai (Julian day 104). The measurements indicate a significant contribution of nitrate to the processed sea salt, which is consistent with the large amounts of supermicron nitrate measured and simulated throughout this period. A large fraction of the particles around Julian day 103 contained aerosol sulfate, coincident with times where distinct plumes of SO_2 were observed and simulated as the ship passed the tip of South Korea. The simulation shows a weaker contribution to sulfate than that observed because

Table 1a. Observed and Simulated Mean Aerosol Submicron Values and Their Correlation Coefficients (R) for TRACE-P All P-3 Flights

	Below 1 km			1 to 3 km			Above 3 km		
Species and Variables	Observed	Modeled	R	Observed	Modeled	R	Observed	Modeled	R
PILS SO_4^{2-}, μg/std m^3	6.3	7.5	0.66	2.6	5.9	0.43	0.50	2.19	0.17
PILS NO_3^-, μg/std m^3	1.7	1.6	0.74	0.99	1.69	0.37	0.35	0.42	−0.19
PILS NH_4^+, μg/std m^3	2.1	2.3	0.73	0.94	2.07	0.29	0.29	0.66	−0.16
PILS K^+, μg/std m^3	0.57	0.25	0.59	0.52	0.19	−0.10	0.34	0.08	0.66
PILS Na^+, μg/std m^3	0.69	0.88	0.44	0.32	0.50	0.14	0.16	0.18	−0.06
PILS Ca^{2+}, μg/std m^3	0.38	0.41	0.18	0.62	0.22	−0.02	0.28	0.20	−0.01
PILS Mg^{2+}, μg/std m^3	0.12	0.10	0.32	0.12	0.05	−0.01	0.082	0.030	−0.06
PILS Cl^-, μg/std m^3	1.38	0.69	0.54	0.76	0.36	0.20	0.61	0.06	0.24

the model predicted a minimum in the sea salt emissions at this time. A quantitative comparison with the ATOFMS data is not possible, as the predicted values represent changes in chloride aerosol mass, while the single particle area ratios are based on the percentage of the number of sea salt particles that indicate reaction with sulfate and nitrate. Further work is needed to develop techniques to more quantitatively compare model results with these exciting and insightful measurements.

[53] The single particle ATOFMS data also provide clear evidence of the chemical interaction among dust, nitrate and sulfate. The percent of the number of supermicron particles that contain nitrate are shown in Figure 15f. The ATOFMS observations show that before the major dust event, most of the coarse mode nitrate was associated with sea salt. During the dusty period (Julian days 102–104), most of the coarse nitrate was associated with dust (over 80%). The predicted nitrate associated with sea salt and dust is also shown in Figure 15f. Shown is the calculated supermicron nitrate mass due to sea-salt interactions (calculated in the absence of dust) and that due to dust interactions (calculated as the difference between the two simulations). The model simulations are qualitatively similar to the ATOFMS percentages, with the simulated nitrate before Julian day 101 dominated by sea salt interactions, and those between Julian days 101 and 104 dominated by interactions with dust. Apparent differences between simulated and observed behavior are found before Julian day 101. However, these differences are due to that the comparison is between percentages of particles and mass. As shown in Figure 15e, the observed mass of sodium is 2 to 10 times higher than calcium. Thus, if these ratios are used to convert the percentages of particles to mass, then the observed curves become much closer to the simulated ones.

4. Discussion

[54] In the cases discussed above various factors were identified that impact the chemical composition and size distribution of inorganic aerosol ions in the east Asia outflow. Asian aerosol contain large amounts of sulfate, nitrate, and ammonium ions, with gradients in the outflow reflecting the spatial distribution of the NO_x, SO_2, and NH_3 emissions and the positions of the springtime cold fronts as they move out and over the western Pacific. The simulation results indicate that the model is able to capture many of the important observed aerosol features. Tables 1a and 1b provide a summary of the observed and simulated values for the inorganic ions for all of the TRACE-P P-3 and ACE-Asia C-130 flights. Since the PILS instrument was used for both the P-3 and C-130 observations, they represent a consistent data set upon which to compare and contrast the two observation periods. Shown are the mean values in three different altitude ranges (i.e., <1 km; 1–3 km; and >3 km). The observations show that in general concentrations are highest in the lowest layer and decrease with altitude. The concentrations of primary species show differences between the two periods, reflecting in large part different source conditions (but with a contribution from different sampling strategies/locations as well; see Figures 2a–2i). For example, potassium is higher in the TRACE-P period reflecting enhanced biomass burning sources (and more frequent flight segments below 30N), while calcium is greater in the ACE-Asia data, reflecting the dust events. The secondary species concentrations are generally higher during the TRACE-P period. The model results show these same features.

[55] When compared to the observations, the model performed best for the lowest altitudes. For example, for the TRACE-P data the simulated mean was within ±30% of the observed values for all species except chloride and potassium (where the model was within a factor of 2). Correlation coefficients ranged from 0.10 to 0.74. In general the predictive skill decreases with altitude (both in terms of mean values and correlations). Similar results were found for the comparison of the model with gaseous species, but in general the simulated gaseous species show higher R values

Table 1b. Observed and Simulated Mean Aerosol Ions and Their Correlation Coefficients (R) for ACE-Asia All C-130 Flights

	Below 1 km			1 to 3 km			Above 3 km		
Species and Variables	Observed	Modeled	R	Observed	Modeled	R	Observed	Modeled	R
PILS SO_4^{2-}, μg/std m^3	4.2	7.1	0.34	2.5	6.0	0.50	0.75	2.92	0.20
PILS NO_3^-, μg/std m^3	1.3	1.2	0.23	0.62	1.46	0.20	0.18	0.55	−0.02
PILS NH_4^+, μg/std m^3	1.3	2.0	0.46	0.70	2.08	0.42	0.15	1.02	0.31
PILS K^+, μg/std m^3	0.38	0.18	0.10	0.20	0.14	0.25	0.15	0.06	−0.01
PILS Na^+, μg/std m^3	0.21	0.40	0.28	0.12	0.19	−0.02	0.089	0.038	−0.09
PILS Ca^{2+}, μg/std m^3	1.16	1.67	0.64	0.65	0.69	0.22	0.42	0.16	0.23
PILS Mg^{2+}, μg/std m^3	0.14	0.18	0.49	0.10	0.08	0.1	0.083	0.018	0.26
PILS Cl^-, μg/std m^3	0.30	0.36	0.55	0.12	0.10	0.05	0.065	0.010	0.20

than those for the aerosol ions as discussed by *Carmichael et al.* [2003a]. Away from the surface the lateral boundary conditions play a larger role. In this regional model the lateral boundary conditions are constant in time and these simulated values show results are less variability at higher altitudes, and this is reflected in the R-values. Interestingly, the performance of the model varied between the two observation periods. For example, the model performed better for potassium during the potassium-rich TRACE-P periods, and calcium predictions improved during the dust-rich ACE-Asia periods. Biases were also observed. The model overestimated sulfate and underestimated potassium. The underestimation of potassium is most likely due to an underestimation of the emissions. The overestimation of sulfate could be due to a variety of factors, including an overestimation of sulfur emissions from the Miyaka-jima volcano [*Carmichael et al.*, 2003b] and/or too large a heterogeneous reaction rate on dust. The fact that sulfate was overestimated during both the dusty and low-dust periods suggests that the bias is not related to the reaction rate on dust.

[56] Further insight into the model performance is found by analyzing the observed and simulated frequency distributions of the submicron ions. The frequency distributions of submicron sulfate, nitrate, ammonium, calcium, and sodium below 1 km are shown in Figure 16. In terms of the observations, the C-130 distributions of sulfate, nitrate, and ammonium are shifted to lower values, while the calcium is shifted to higher values relative to the P-3 distributions. This behavior again reflects the influence of dust on the size distribution of the inorganic aerosol ions. The model frequency distributions follow closely the observed distributions for nitrate, ammonium, and calcium. In the case of sulfate the simulated frequency is shifted to higher concentrations.

[57] The above comparisons indicate that the simulated dust (as implied by the calcium values) is well captured in the analysis. This is important as the model results are very sensitive to the calcium amount and size distribution. Simulated sea salt as inferred from sodium values is predicted within a factor of 2 of the observations, with a tendency to underestimate the coarse fraction (not shown). These results also suggest that the model captures the main features in ammonium and nitrate, but may underpredict the fraction of sulfate in the supermicron mode. However, due to the differences in the measurement methods and the limited number of TAS samples, these finding must be viewed with caution.

[58] Enhanced levels of dust are found in the east Asia outflow during the spring, and its presence has a profound influence on the aerosol composition. One of the major impacts of dust is to modify the size distributions of sulfate and nitrate. To characterize this influence, we present the relationship between sulfate and nitrate coarse ratios for the dust events encountered by the C-130 flights during ACE-Asia. In this analysis we identified the individual measurements in the 3-min merged data set that were heavily influenced by dust. We defined a dust-impacted sample as one in which the simulated total dust was greater than 100 $\mu g/m^3$ in standard state, as discussed in detail by *Tang et al.* [2004a]. For these observation points we calculated the sulfate and nitrate coarse fractions using the MOI data. These ratios are shown in Figure 17. Since the number of MOI observations was relatively few (due to sampling times), the data in Figure 17a are sparse. The data points are color-coded by the observed total calcium amounts as determined by TAS. The calculated coarse ratios, color-coded by the simulated total calcium levels, are also presented (Figure 17b). The number of points used in the model analysis is large, reflecting that in the model we have fine and coarse predictions for every identified 3-min sample. We see that when dust (calcium) loadings are low, sulfate resides mainly in the fine mode and nitrate is driven into the coarse mode. This situation also appeared in the TRACE-P flight analysis (not shown). The partitioning of nitrate is also affected by the ambient NH_3 concentrations. If NH_3 concentrations are in excess of that needed to neutralize sulfate, then NH_4NO_3 can exist in the fine mode, even in the presence of dust. So, for a certain calcium loading, the nitrate coarse ratio (and to a lesser extent sulfate) can exhibit a high degree of variability, as indicated by the banded areas (Figure 17). Within these bands the nitrate coarse ratios decrease as the ammonia levels increase. As the dust loading increases, the coarse ratio of nitrate decreases, while that for sulfate increases, and the variability in the ratios decreases. Both predictions and measurements show that sulfate and nitrate coarse ratios approach a point that is associated with the dust coarse fraction. In the observations, this convergence point corresponds to nitrate and sulfate coarse fractions of 0.6 and 0.5, respectively. In the model the convergence values are lower, 0.4 and 0.3, respectively. It should be emphasized that the observed coarse ratios are highly uncertain, and that a consistent picture does not emerge when the various measurement techniques are combined; i.e., PILS, TAS, MOI, etc. This is an area that requires further effort.

[59] The convergence values are determined by the properties of the dust; the key aspects being the dust size distribution (coarse fraction) and the reactivity of the particles with respect to sulfate and nitrate (with the amount of reactive/available/soluble calcium being the critical factor/surrogate). In the model simulations the emitted dust has a coarse fraction of $\sim$0.8, with 20% of the calcium in the coarse mode available for reaction. Sensitivity studies show that increasing the coarse fraction, or increasing the reactive available calcium, shifts the convergence point to larger values. Further studies are needed to reduce the uncertainties in the measured values, as these ratios provide an important constraint to the model.

[60] The behavior shown in Figure 17 reflects the interaction of dust with the secondary inorganic ions. In the absence of dust, sulfate is formed by nucleation processes, which produce small particles (a low coarse fraction). The cation and anion balance among sulfate, ammonium, and other ions determines how nitrate is distributed in size. In the absence of dust, then the availability of ammonia will determine, along with temperature and relative humidity, whether fine mode nitrate forms. The appearance of dust provides the opportunity for sulfate (and SO_2) and nitrate (and NO_x) to directly interact with the surface. In the case of sulfur dioxide, these interactions result in the enhancement of the sulfate coarse ratio, and the coarse fraction of sulfate increases with increasing amounts of dust as shown in Figure 17. In an SO_2-only system with sufficiently high dust loadings so that the formation of fine mode sulfate by

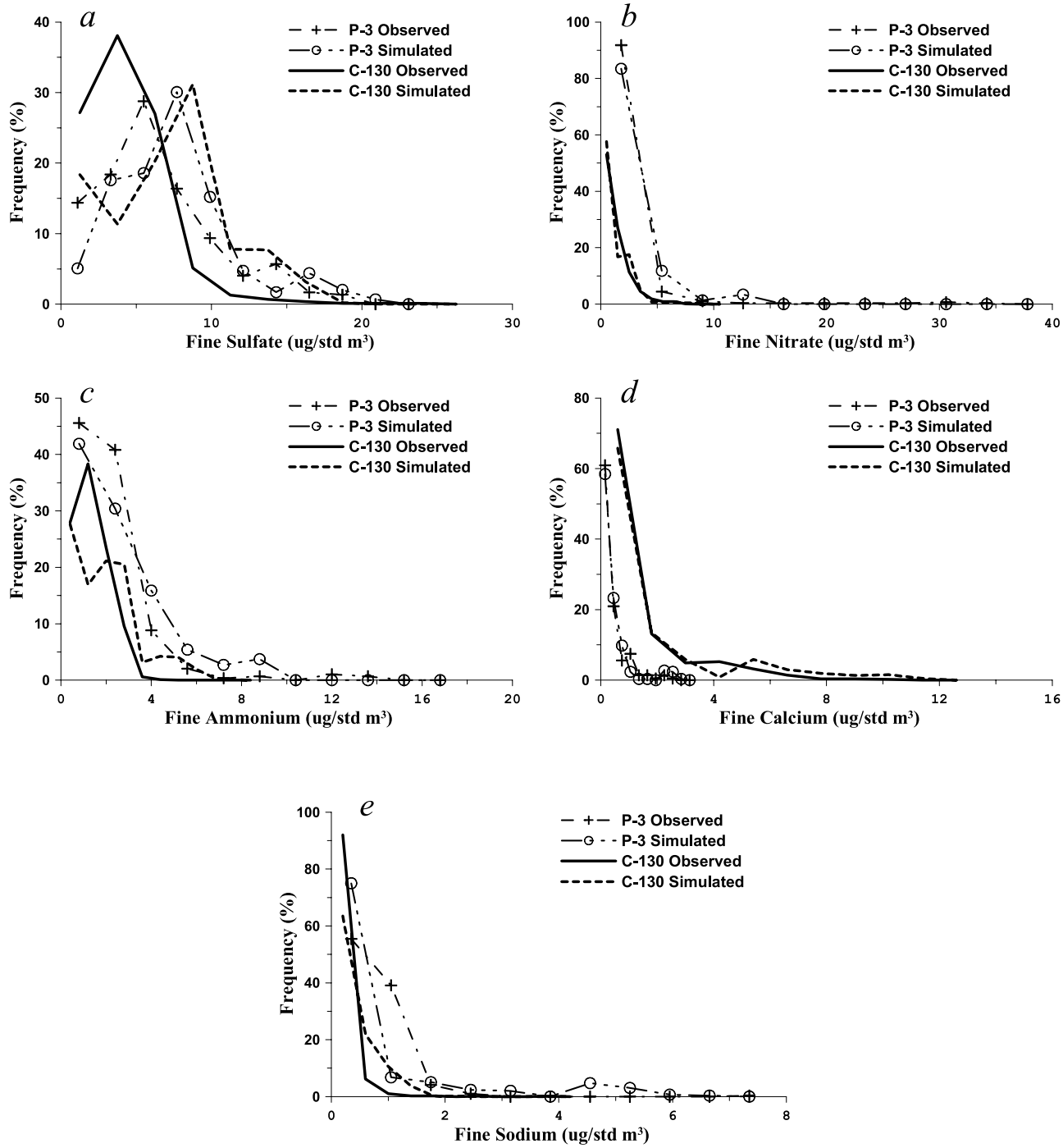

Figure 16. Simulated and observed frequency distributions (%) of fine aerosol concentrations below 1 km for all TRACE-P P-3 and ACE-Asia C-130 flights: (a) sulfate, (b) nitrate, (c) ammonium, (d) calcium, and (e) sodium.

nucleation can be neglected, the steady state value for the coarse ratio of sulfate becomes the coarse fraction of the reactive surface. The actual value is lower than this as nitrate competes for the reactive surface. In contrast, in a sulfur-rich and ammonia-limited environment nitrate cannot form in the fine mode. Thus, at very low dust levels, the fine mode is acidic, and nitrate is partitioned exclusively into the coarse mode. As ammonia levels increase, fine mode nitrate forms, and the coarse fraction decreases. Furthermore, dust in the fine mode provides alkaline ions to help neutralize the acidity of sulfate, which also allows for nitrate uptake in the fine mode. This leads to a decrease in the nitrate coarse fraction as dust levels increase, as shown in Figure 17. In a pure nitric acid environment dominated by dust, the steady state coarse fraction of nitrate would converge to the value of the dust reactive coarse fraction. Under these conditions, the role of ammonia is minimal, and the variability of the coarse dust fraction of nitrate is small. In the actual

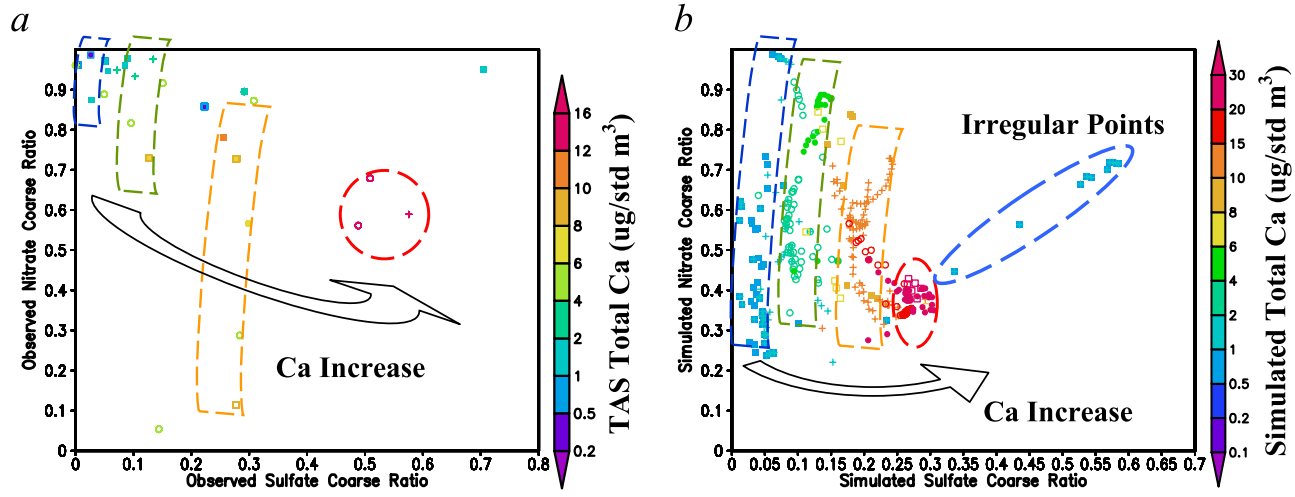

Figure 17. (a) Observed and (b) simulated sulfate coarse ratio versus nitrate coarse ratio for dust events (simulated dust >100 μg/m^3) of all C-130 flights [*Tang et al.*, 2004a] colored in total calcium concentrations. Observed coarse ratios were measured with MOI instrument. All data come from 3-min merged data set.

atmosphere, the values for the coarse fractions of nitrate and sulfate are lower than the reactive coarse fraction, as the dust simultaneously accommodates all the reactive species.

[61] Figure 17 also shows that some of the predictions do not follow the trends discussed above. For these points, nitrate and sulfate coarse ratios are linearly related. The data in Figure 17b are replotted with a classification using the coarse dust fresh ratio (equation (1)) in Figure 18. When the dust is well aged (coarse dust fresh ratios less than 0.2), the sulfate coarse ratio increases and the nitrate coarse ratio decreases, as discussed above. However, when the dust is fresh (coarse dust fresh ratio >0.4), surface saturation effects do not limit the uptake of nitric acid and sulfur dioxide from the gas phase. Since the total surface area available for uptake is largest in the coarse mode, simultaneous sorption of these gases increases the coarse fraction of sulfate and nitrate. These results show that when dust is very fresh, nitrate and sulfate formation are driven by the same mechanism (but with HNO_3 uptake occurring at a faster rate than SO_2), which leads to their positively correlated coarse ratios. However, the correlation slope is not a fixed value, but depends on the ambient NO_2, HNO_3, and SO_2 concentrations. These results point to the need to measure the dust fresh ratio (and carbonate).

[62] The large-scale influence of the dust on the partitioning of the semivolatile ions, nitrate and ammonium is shown in Figure 19 where the weekly averaged molar ammonia aerosol ratio ($NH_4/(NH_3 + NH_4)$) and the molar nitrate aerosol ratio ($NO_3/(HNO_3 + NO_3^-)$) are plotted. The distributions of the ammonia aerosol ratio are similar for these two periods over land, where ammonia emissions are very high. When the aerosol-rich air mass is transported over the ocean, the ratio increases as ammonia partitions into the aerosol phase. However, the extent of the increase differs for these two periods. The low-dust period shows a faster aerosol-ratio enhancement than the heavy-dust period. Over the Yellow Sea and the East China Sea, the low-dust period has broad areas where the ammonia aerosol ratio >0.6, but during the heavy-dust period this ratio was usually less than 0.5. As discussed previously, dust tends to decrease the ammonia aerosol ratio, but increase the nitrate aerosol ratio. During March 13–19 a broad area in the western Pacific had nitrate aerosol ratios less than 0.3, due to the SO_2 oxidization under the cation-stable condition, as discussed in section 3.1. During the heavy-dust period this area with small nitrate aerosol ratios nearly disappeared. Over land the dust storms extended the area with nitrate aerosol ratios >0.9. These results indicate that ammonia emissions in large portions of east Asia are in excess of those needed to neutralize sulfate and nitrate, and that significant amounts of gas-phase ammonia exist. Therefore, to close the budget of ammonia (and to test/constrain ammonia emissions), it is necessary to measure gas-phase ammonia. These results are in general agreement with recent gaseous ammonia mea-

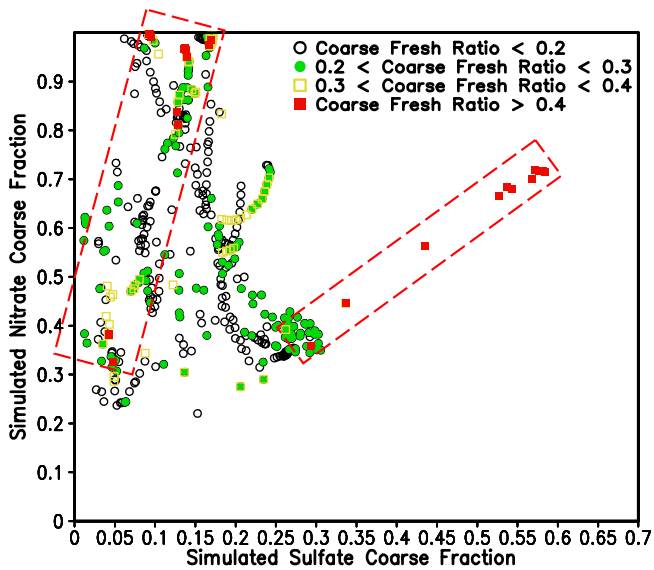

Figure 18. Same as Figure 17b, but grouped by simulated coarse dust fresh ratio.

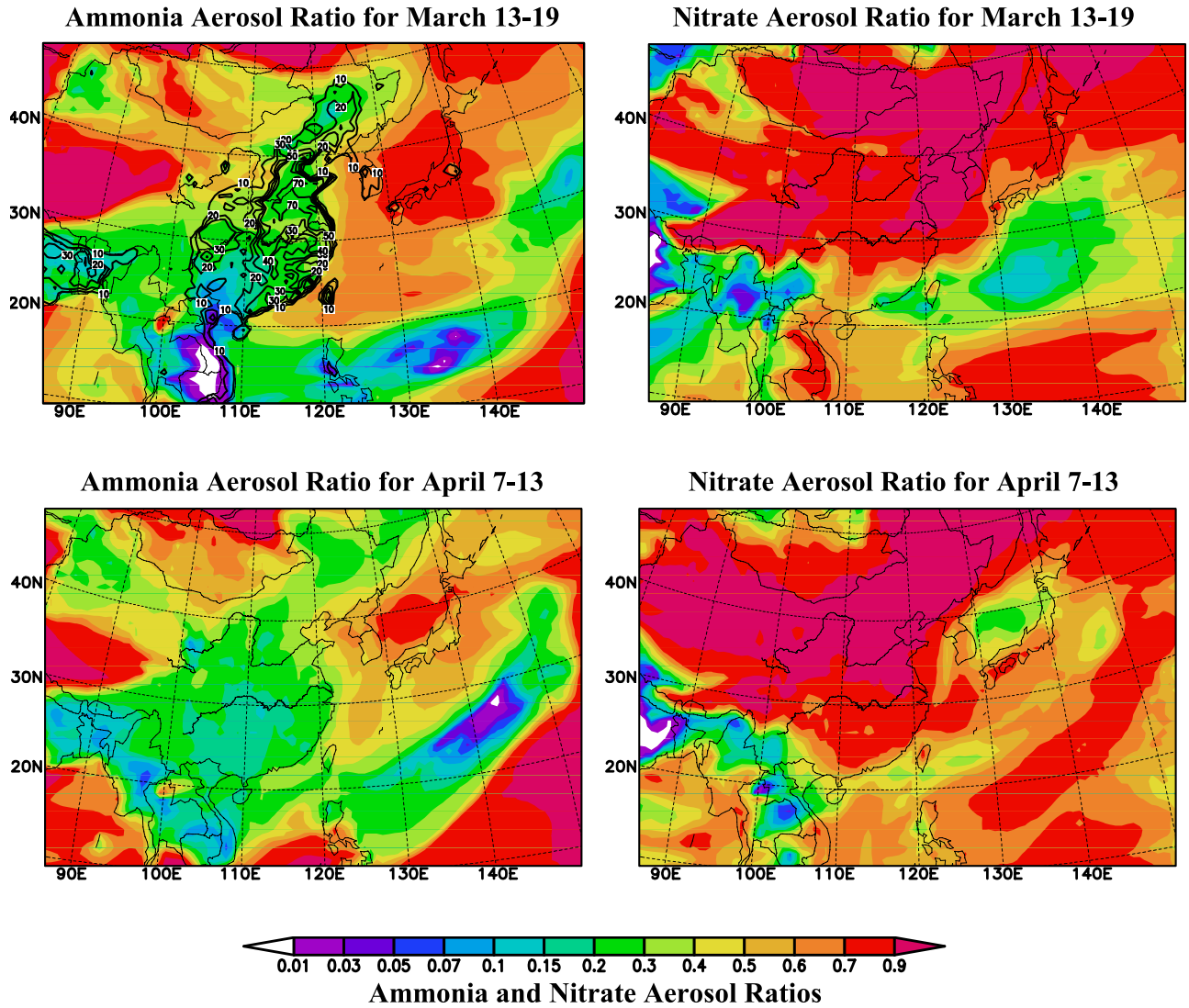

Figure 19. Simulated averaged ammonia and nitrate aerosol ratios in 400 m level for the periods of March 13–19, and April 7–13. Ammonia emissions estimated by *Streets et al.* [2003] are plotted by contour line in top left panel in unit mole/hr/km^2.

surements in Asia conducted using diffusive samplers [*Carmichael et al.*, 2003c], where ammonia levels in the spring in eastern China were found to exceed 5 ppb.

[63] As discussed throughout this paper, dust has a significant impact on the aerosol composition. Some secondary aerosol processes are reversible, like ammonium uptake. When dust is introduced, the alkalinity increases and ammonium can partition back into gaseous ammonia. Other processes are irreversible, for example, sulfate nucleation and SO_2-dust heterogeneous reactions. From an analysis perspective it is interesting to see the extent to which a three-dimensional framework is needed to represent the aerosol composition as a function of size. To study this, we performed two box-model simulations. The aerosol mechanisms in the box model are identical to those in the 3-D model. The box model was run for each point along the C-130 flight track. In box-model A the initial conditions for each point were extracted from the 3-D with-dust simulation, but dust and associated calcium and magnesium ions were set to zero (same as the 3-D without-dust simulation). The box-model B has dust and associated ions from the 3-D with-dust simulation, but its other inputs came from the 3-D without-dust simulation. The models were then run to equilibrium. These two box-model simulations represent the situation of in situ switching of dust loadings between the 3-D with and without dust simulations.

[64] Figure 20 shows the simulation comparisons for nitrate and ammonium along the C-130 flight 6. The 3-D with-dust prediction agrees best with the ammonium, and the three-dimensional without-dust simulation overestimated both fine and total ammonium. The two box-model simulations yielded ammonium concentrations between these 3-D simulations. After removing dust, the box-model A simulation produced ammonium concentrations higher than the with-dust calculation, because removing calcium leaves more room for ammonium uptake. However, the values produced were still lower than the 3-D without-dust simulation. Results from box-model B show a reduction in

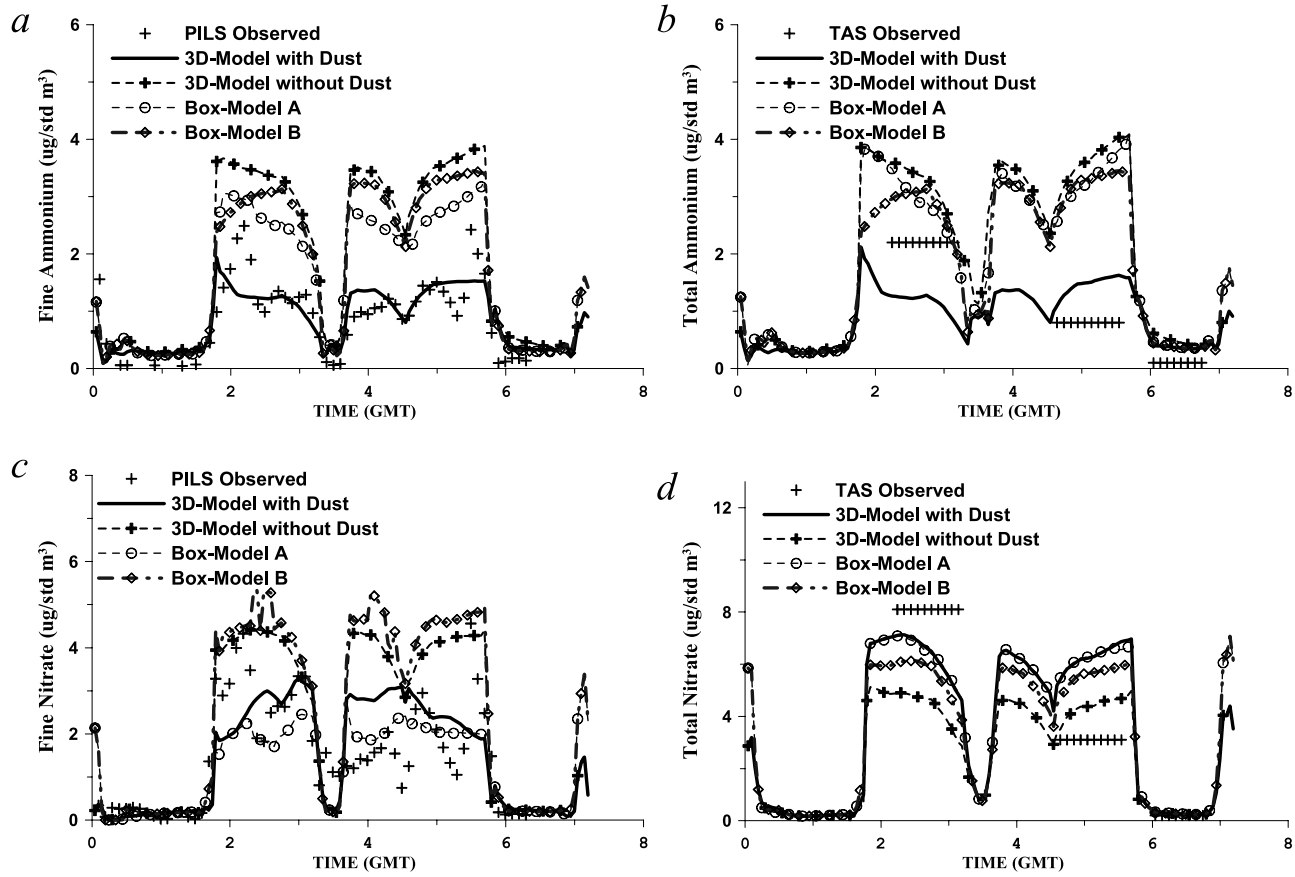

Figure 20. Simulated submicron and total ammonium and nitrate calculated with different box and 3-D model configurations for the C-130 flight.

fine and total ammonium from the 3-D without-dust simulation, but with values higher than those for the 3-D with-dust simulation. The box-model runs clearly show the same tendencies as the corresponding 3-D calculations. It should be noted that C-130 flight 6 mostly encountered ammonia-rich airm asses in the low altitudes. Even under these conditions, this sensitivity study shows that the dust impacts on aerosol equilibrium processes are not fully revealed by the in situ examination, since the aerosol status is relative to its time history. This is illustrated further by looking at nitrate. The 3-D with-dust simulation yielded low HNO_3 levels for the conditions along this flight, but the 3-D without-dust simulation produced appreciable amounts of HNO_3, so box-model B shows that nitrate increased when dust was inserted (Figures 20c and 20d). This enhancement occurred in both the fine and coarse modes. Box-model A produced nearly the same total nitrate as the 3-D with-dust simulation, but significantly less fine nitrate. This means that when removing dust calcium, nitrate was repelled from fine mode into the coarse mode. This study shows that the box model results for semivolatile ions can differ significantly from the 3-D simulations. For sulfate these box-model runs produced nearly the same results as their 3-D counterpart. The aerosol sampled by the aircrafts reflected the results of four-dimensional interactions, including the air mass journey, history, and associated situation of gaseous species. These interactions, including heterogeneous uptake, are too complex to be fully represented by in situ examinations in this complex situation of Asian outflow. These results further illustrate the difficulty of simulating the aerosol composition in the presence of dust, due in large part to the difficulties in predicting the dust emissions and initial composition.

[65] A key issue that remains to be resolved is the extent to which the calcium carbonates in the dust participate in aerosol chemistry. Unfortunately, direct measurements of carbonates were not available during these experiments. In this paper we assumed that only a fraction of the carbonates were active (as discussed in section 2.1). The analysis of the PILS instrument by Maxwell-Meier et al. (submitted manuscript, 2003) infers that appreciable amounts of carbonates were still in the bulk aerosol. They estimated aerosol carbonate as the difference between the measured cations and anions. These values were found to be well correlated with measured calcium and magnesium (as expected if the carbonate was associated with the dust) as shown in Figure 21. The points with negative values on the y-axis (in both the observations and the simulations) occur for highly processed sea salt that is deficient in chloride. The model-calculated total carbonate (sum of inactive/inaccessible carbonate and active carbonate remaining in the particle) in the submicron particles are also plotted in Figure 21 for comparison. The model values are in quantitative agreement with the "observed" values. While this comparison indicates that the assumptions used in this paper constrain the active carbonate in a manner consistent with

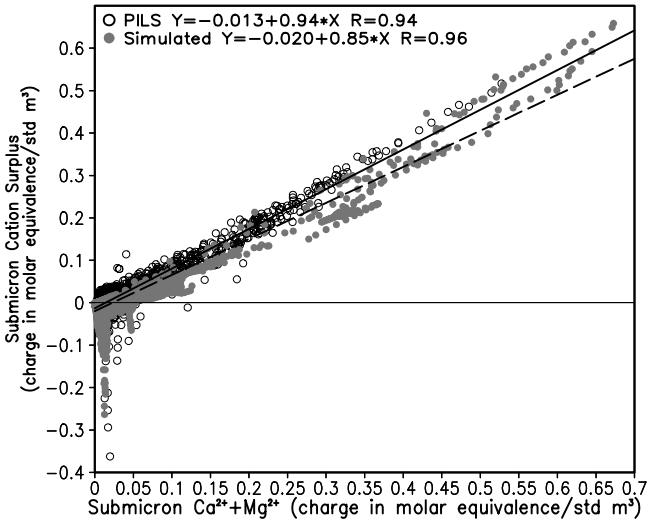

Figure 21. Simulated and observed correlations of cation surplus (cation charges minus anion charges) versus sum of calcium and magnesium in fine mode for all ACE-Asia C-130 flights.

the observations, more work is needed to determine the fundamental processes at play.

5. Conclusions

[66] In this paper, the three-dimensional regional scale model STEM-2K3 that incorporated an on-line, size-resolved, aerosol thermodynamics model (SCAPE-II), was used to study the aerosol ion distributions, and factors that influence the composition-size relationships, in the east Asia outflow during the TRACE-P and ACE-Asia periods. Results from the model were compared with various observations, and used to study how the inorganic aerosol composition changed as air masses travel off the continent and out over the western Pacific.

[67] The Asian outflow during March and April of 2001 was heavily polluted with high-aerosol loading. In this region, both primary and secondary aerosols contribute to the pollution. During this period, dust storms and biomass burning contributed in important ways to the aerosol loadings of the outflow. Dust was shown to have a major impact on the amount and size distribution of secondary inorganic aerosol ions. In the absence of dust, nucleation plays the main role in sulfate formation, and produces fine mode sulfate. In addition it was found that throughout much of east Asia ammonia emissions are sufficiently large to accommodate both fine-mode sulfate and nitrate.

[68] Dust was shown to strongly affect the aerosol ions and their size distributions. Results from this study indicated that dust alters the partitioning of the semivolatile components between the gas and aerosol phases as well as the size distributions of the secondary aerosol constituents. A main role of dust in the equilibrium process is through the enhancement of the aerosol calcium concentration, which shifts the equilibrium balance to an anion-limited status. This status benefits the uptake of sulfate and nitrate, but repels ammonium. Surface reactions on dust provide an additional mechanism to produce aerosol nitrate and sulfate. The size distribution of dust was shown to be a critical factor. As much of the dust mass resides in the coarse mode (70–90%), appreciable amounts of sulfate and nitrate are in the supermicron particles. For sulfate the observations and the analysis indicate that 10–30% of sulfate was in the coarse fraction. In the case of nitrate more than 80% was found in the coarse fraction. The strength of dust influence was shown to be determined by its fresh ratio and concentration.

[69] The results of this paper also point out remaining issues and challenges for the model and measurements. From the modeling perspective the results were found to be very sensitive to the dust mass, its size distribution, assumptions about its extent of equilibrium involvement, and the fraction of the aerosol mass available for reaction. Estimating dust mass and size distributions using emission models is fraught with uncertainty (as discussed by *Kline et al.* [2004]). Results obtained in ACE-Asia and TRACE-P have allowed for more rigorous evaluation of model prediction of dust, and provided more details into the dust size distribution. As a result, we have improved our ability to estimate dust emissions in east Asia; but quantitative, episodic, and predictive capabilities remain a challenge.

[70] The issue of how to characterize the chemically active portion of the aerosol presents a challenge. This modeling study (as well as Song et al. (submitted manuscript, 2003)) suggests that an appreciable fraction of the calcium in the aerosol in the outflow may be chemically inactive (or externally mixed). Quantifying the chemical activity state from the observations is difficult, and cannot be determined by composition measurements by themselves. Microscopy and single particle techniques provide important information. At present the information provided from the single particle statistics derived from particle numbers and the model mass-based predicts do not correspond. Results presented in this paper show how these can be used together to provide useful information and aid in the interpretation, but ways to facilitate more quantitative comparisons need to be found.

[71] The submicron and supermicron fractions of key ions provide valuable information to constrain and test our understanding of aerosol processes. For example, the sulfate and nitrate coarse fractions are dependent on the characteristics of the dust, surface chemistry, the chemical age of the particle, among other factors. However, ACE-Asia and TRACE-P observations remind us that quantifying these ratios is also difficult (due to differences in inlets, collection efficiencies, sampling times, artifacts, etc.).

[72] The aerosol observed by the mobile platforms, which usually operated downwind of the major sources and over the sea, was different from that over the source regions. As discussed in detail in this paper, the aerosol in the outflow was chemically aged and modified by dust and sea salt. Quantifying the aging processes is important in the interpretation of the data, and in the development of a predictive capability of characterizing aerosol composition and size. In the case of dust, aerosol carbonate is an important parameter. Large quantities are expected (and inferred from observations; see Maxwell-Meier et al. (submitted manuscript, 2003)) in the Asian aerosol, but there were few

carbonate measurements obtained in these experiments. The single particle observations provide direct information on aerosol chemistry (e.g., sea salt and dust interactions as discussed in this paper), but as discussed above, we need to more deeply mine the information provided by the measurements and the models.

[73] The chemical interaction between primary aerosol and reactive gases in the Asian outflow also may lead to important changes in the aerosol optical properties in east Asia. For example, Asian dust and sulfate are reflective aerosols. Sulfate generated from ordinary nucleation is concentrated in the fine mode. However, as discussed in this paper, when dust is mixed with anthropogenic pollutants the sulfate total mass can increase through SO_2 heterogeneous uptake. The net effect on optical depth is not proportional to the increase in total sulfate, as a fraction of the increased sulfate will reside the coarse mode. At the same time, the optical properties of dust change as the dust chemically ages and its surface becomes contaminated by sulfate and nitrate. These interactions change the aerosol mixing state and size distributions, which in turn alters their optical properties. These issues are discussed in more detail by *Clarke et al.* [2004]. The modeled fields discussed in this paper were used to estimate aerosol radiative forcing in east Asia as discussed by *Conant et al.* [2003].

[74] The interaction among aerosol ions and gaseous pollutant also shows significant impact on gas-phase chemistry. *Tang et al.* [2004a] discussed the dust heterogeneous influence on gaseous chemistry. The HNO_3-nitrate equilibrium process is another example how aerosol process affects gaseous species. Recent studies, such as *Tang et al.* [2004b], indicate significant NO_y loss during the transpacific transport, which we associate with aerosol-gas interaction.

[75] The results presented in this paper suggest that present day atmospheric models have substantial interpretive and diagnostic capabilities. However, the results presented here also point out that improvement in our predictive capability will require substantial reductions in uncertainties. Continued integration of models and measurements is clearly needed. Finally, the analysis presented here was restricted to inorganic aerosol. It is important to extend this analysis to include interaction with carbonaceous aerosol, and this will be the subject of a future paper.

[76] **Acknowledgments.** We appreciate Marco Rodriguez (University of California at Irvine) for his help on the SCAPE source code conversion. This work was supported in part by grants from the NSF Atmospheric Chemistry Program, NSF grant Atm-0002698, NASA GTE and ACMAP programs, and the Department of Energy Atmospheric Chemistry Program. This work (Itsushi Uno) was also partly supported by Research and Development Applying Advanced Computational Science and Technology (ACT-JST) and the CREST of Japan Science and Technology Corporation. Barry Huebert's contribution to this work was supported by National Science Foundation grants ATM0002698 and ATM0002604. This research is a contribution to the International Global Atmospheric Chemistry (IGAC) Core Project of the International Geosphere Biosphere Program (IGBP) and is part of the IGAC Aerosol Characterization Experiments (ACE).

References

Bahreini, R., J. L. Jimenez, J. Wang, R. C. Flagan, J. H. Seinfeld, J. T. Jayne, and D. R. Worsnop (2003), Aircraft-based aerosol size and composition measurements during ACE–Asia using an Aerodyne aerosol mass spectrometer, *J. Geophys. Res.*, *108*(D23), 8645, doi:10.1029/2002JD003226.

Bates, T. S., et al. (2004), Marine boundary layer dust and pollutant transport associated with the passage of a frontal system over eastern Asia, *J. Geophys. Res.*, doi:10.1029/2003JD004094, in press.

Carmichael, G. R., et al. (2003a), Regional-scale chemical transport modeling in support of the analysis of observations obtained during the TRACE-P experiment, *J. Geophys. Res.*, *108*(D21), 8823, doi:10.1029/2002JD003117.

Carmichael, G. R., et al. (2003b), Evaluating regional emission estimates using the TRACE-P observations, *J. Geophys. Res.*, *108*(D21), 8810, doi:10.1029/2002JD003116.

Carmichael, G. R., M. Ferm, N. Thongboonchoo, J.-H. Woo, L. Y. Chan, and K. Murano (2003c), Measurements of sulfur dioxide, ozone, and ammonia concentrations in Asia, Africa, and South America using passive samplers, *Atmos. Environ.*, *37*, 1293–1308.

Carter, W. (2000), Documentation of the SAPRC-99 chemical mechanism for VOC reactivity assessment, final report to California Air Resources Board, contract 92–329, Univ. of Calif., Riverside, 8 May.

Chin, M., P. Ginoux, R. Lucchesi, B. Huebert, R. Weber, T. Anderson, S. Masonis, B. Blomquist, A. Bandy, and D. Thornton (2003), A global aerosol model forecast for the ACE-Asia field experiment, *J. Geophys. Res.*, *108*(D23), 8654, doi:10.1029/2003JD003642.

Clarke, A. D., et al. (2004), Size distributions and mixtures of dust and black carbon aerosol in Asian outflow: Physiochemistry and optical properties, *J. Geophys. Res.*, *109*, D15S09, doi:10.1029/2003JD004378.

Conant, W. C., J. H. Seinfeld, J. Wang, G. R. Carmichael, Y. Tang, I. Uno, P. J. Flatau, K. M. Markowicz, and P. K. Quinn (2003), A model for the radiative forcing during ACE-Asia derived from CIRPAS Twin Otter and R/V *Ronald H. Brown* data and comparison with observations, *J. Geophys. Res.*, *108*(D23), 8661, doi:10.1029/2002JD003260.

Dentener, F. J., G. R. Carmichael, Y. Zhang, J. Lelieveld, and P. J. Crutzen (1996), Role of mineral aerosol as a reactive surface in the global troposphere, *J. Geophys. Res.*, *101*, 22,869–22,889.

Dibb, J. E., R. W. Talbot, E. Scheuer, G. Seid, M. Avery, and H. B. Singh (2003), Aerosol chemical composition in Asian continental outflow during the TRACE-P campaign: Comparison with PEM-West B, *J. Geophys. Res.*, *108*(D21), 8815, doi:10.1029/2002JD003111.

Gard, E., et al. (1997), Real-time analysis of individual atmospheric aerosol particles: Design and performance of a portable ATOFMS, *Anal. Chem.*, *69*(20), 4083–4091.

Gong, S. L., X. Y. Zhang, T. L. Zhao, I. G. McKendry, D. A. Jaffe, and N. M. Lu (2003), Characterization of soil dust aerosol in China and its transport and distribution during 2001 ACE-Asia: 2. Model simulation and validation, *J. Geophys. Res.*, *108*(D9), 4262, doi:10.1029/2002JD002633.

Goodman, A. L., G. M. Underwood, and V. H. Grassian (2000), A laboratory study of the heterogeneous reaction of nitric acid on calcium carbonate particles, *J. Geophys. Res.*, *105*, 29,053–29,064.

Goodman, A. L., P. Li, C. R. Usher, and V. H. Grassian (2001), Heterogeneous uptake of sulfur dioxide on aluminum and magnesium oxide particles, *J. Phys. Chem. A*, *105*, 6109–6120.

Guazzotti, S. A., et al. (2003), Characterization of carbonaceous aerosols outflow from India and Arabia: Biomass/biofuel burning and fossil fuel combustion, *J. Geophys. Res.*, *108*(D15), 4485, doi:10.1029/2002JD003277.

Hanisch, F., and J. N. Crowley (2001), Heterogeneous reactivity of gaseous nitric acid on Al_2O_3, $CaCO_3$, and atmospheric dust samples: A Knudsen cell study, *J. Phys. Chem. A*, *105*, 3096–3106.

Huebert, B. J., T. Bates, P. B. Russell, G. Shi, Y. J. Kim, K. Kawamura, G. R. Carmichael, and T. Nakajima (2003), An overview of ACE-Asia: Strategies for quantifying the relationships between Asian aerosols and their climatic impacts, *J. Geophys. Res.*, *108*(D23), 8633, doi:10.1029/2003JD003550.

Jacob, D. J. (2000), Heterogeneous chemistry and tropospheric ozone, *Atmos. Environ.*, *34*, 2131–2159.

Jacob, D. J., J. H. Crawford, M. M. Kleb, V. S. Connors, R. J. Bendura, J. L. Raper, G. W. Sachse, J. C. Gille, L. Emmons, and C. L. Heald (2003), Transport and Chemical Evolution Over the Pacific (TRACE-P) aircraft mission: Design, execution, and first results, *J. Geophys. Res.*, *108*(D20), 9000, doi:10.1029/2002JD003276.

Jordan, C. E., J. E. Dibb, B. E. Anderson, and H. E. Fuelberg (2003a), Uptake of nitrate and sulfate on dust aerosols during TRACE-P, *J. Geophys. Res.*, *108*(D21), 8817, doi:10.1029/2002JD003101.

Jordan, C. E., et al. (2003b), Chemical and physical properties of bulk aerosols within four sectors observed during TRACE-P, *J. Geophys. Res.*, *108*(D21), 8813, doi:10.1029/2002JD003337.

Kim, Y. P., and J. H. Seinfeld (1995), Atmospheric gas-aerosol equilibrium III: Thermodynamics of crustal elements Ca^{2+}, K^+, Mg^{2+}, *Aerosol Sci. Technol.*, *22*, 93–110.

Kim, Y. P., J. H. Seinfeld, and P. Saxena (1993a), Atmospheric gas-aerosol equilibrium I: Thermodynamic model, *Aerosol Sci. Technol.*, *19*, 151–181.

Kim, Y. P., J. H. Seinfeld, and P. Saxena (1993b), Atmospheric gas-aerosol equilibrium II: Analysis of common approximations and activity coefficient calculation methods, *Aerosol Sci. Technol.*, *19*, 182–198.

Kline, J., B. Huebert, S. Howell, B. Blomquist, J. Zhuang, T. Bertram, and J. Carrillo (2004), Aerosol composition and size versus altitude measured from the C-130 during ACE-Asia, *J. Geophys. Res.*, doi:10.1029/2004JD004540, in press.

Lee, Y. N., et al. (2003), Airborne measurement of inorganic ionic components of fine aerosol particles using the PILS-IC technique during ACE-Asia and TRACE-P, *J. Geophys. Res.*, *108*(D23), 8646, doi:10.1029/2002JD003265.

Ma, Y., et al. (2003), Characteristics and influence of biosmoke on the fine-particle ionic composition measured in Asian outflow during the Transport and Chemical Evolution Over the Pacific (TRACE-P) experiment, *J. Geophys. Res.*, *108*(D21), 8816, doi:10.1029/2002JD003128.

Michel, A. E., C. R. Usher, and V. H. Grassian (2002), Heterogeneous and catalytic uptake of ozone on mineral oxides and dust: A Knudsen cell investigation, *Geophys. Res. Lett.*, *29*(14), 1665, doi:10.1029/2002GL014896.

Mori, I., M. Nishikawa, T. Tanimura, and H. Quan (2003), Change in size distribution and chemical composition of Kosa aerosol during long range transport, *Atmos. Environ.*, *37*, 4253–5263.

Phadnis, M. J., and G. R. Carmichael (2000), Influence of mineral aerosol on the tropospheric chemistry of east Asia, *J. Atmos. Chem.*, *36*, 285–323.

Prather, K. A., et al. (1994), Real-time characterization of individual aerosol particles using time-of-flight mass spectrometry, *Anal. Chem.*, *66*(9), 1403–1407.

Prince, A. P., J. L. Wade, V. H. Grassian, P. D. Kleiber, and M. A. Young (2002), Heterogeneous reactions of soot aerosols with nitrogen dioxide and nitric acid studied in an atmospheric chamber, *Atmos. Environ.*, *36*, 5729–5740.

Quinn, P. K., et al. (2000), Surface submicron aerosol chemical composition: What fraction is not sulfate?, *J. Geophys. Res.*, *105*(D5), 6785–6805.

Seinfeld, J. H., et al. (2004), Regional climatic and atmospheric chemical effects of Asian dust and pollution, *Bull. Am. Meteorol. Soc.*, in press.

Song, C. H., and G. R. Carmichael (2001), A three-dimensional modeling investigation of the evolution processes of dust and sea-salt particles in east Asia, *J. Geophys. Res.*, *106*, 18,131–18,154.

Streets, D. G., et al. (2003), An inventory of gaseous and primary aerosol emissions in Asia in the year 2000, *J. Geophys. Res.*, *108*(D21), 8809, doi:10.1029/2002JD003093.

Tang, Y., et al. (2003a), Impacts of aerosols and clouds on photolysis frequencies and photochemistry during TRACE-P: 2. Three-dimensional study using a regional chemical transport model, *J. Geophys. Res.*, *108*(D21), 8822, doi:10.1029/2002JD003100.

Tang, Y., et al. (2003b), Influences of biomass burning during the Transport and Chemical Evolution Over the Pacific (TRACE-P) experiment identified by the regional chemical transport model, *J. Geophys. Res.*, *108*(D21), 8824, doi:10.1029/2002JD003110.

Tang, Y., et al. (2004a), Impacts of dust on regional tropospheric chemistry during the ACE-Asia experiment: A model study with observations, *J. Geophys. Res.*, *109*, D19S21, doi:10.1029/2003JD003806.

Tang, Y., et al. (2004b), Multiscale simulations of tropospheric chemistry in the eastern Pacific and on the U. S. West Coast during spring 2002, *J. Geophys. Res.*, *109*, D23S11, doi:10.1029/2004JD004513.

Underwood, G. M., C. H. Song, M. Phadnis, G. R. Carmichael, and V. H. Grassian (2001), Heterogeneous reactions of NO_2 and HNO_3 on oxides and mineral dust: A combined laboratory and modeling study, *J. Geophys. Res.*, *106*, 18,055–18,066.

Usher, C. R., H. Al-Hosney, S. Carlos-Cuellar, and V. H. Grassian (2002), A laboratory study of the heterogeneous uptake and oxidation of sulfur dioxide on mineral dust particles, *J. Geophys. Res.*, *107*(D23), 4713, doi:10.1029/2002JD002051.

Whitby, K. T. (1978), The physical characteristics of sulfur aerosols, *Atmos. Environ.*, *12*, 135–159.

Woo, J.-H., et al. (2003), Contribution of biomass and biofuel emissions to trace gas distributions in Asia during the TRACE-P experiment, *J. Geophys. Res.*, *108*(D21), 8812, doi:10.1029/2002JD003200.

Zhang, Y., and G. R. Carmichael (1999), The role of mineral aerosol in tropospheric chemistry in east Asia—A model study, *J. Appl. Meteorol.*, *38*, 353–366.

G. R. Carmichael, V. H. Grassian, Y. Tang, J.-H. Woo, and J. J. Yienger, Center for Global and Regional Environmental Research, University of Iowa, Iowa City, IA 52242, USA. (ytang@cgrer.uiowa.edu)

A. D. Clarke and B. Huebert, School of Ocean and Earth Science and Technology, University of Hawaii, Honolulu, HI 96822, USA.

D. Dabdub, Department of Mechanical and Aerospace Engineering, University of California, Irvine, CA 92717, USA.

J. E. Dibb and R. W. Talbot, Department of Earth Sciences, University of New Hampshire, Durham, NH 03824, USA.

S. A. Guazzotti, K. A. Prather, and D. A. Sodeman, Department of Chemistry and Biochemistry, University of California, San Diego, CA 92037, USA.

J. E. Johnson and P. K. Quinn, Pacific Marine Environmental Laboratory, NOAA, Seattle, WA 98115, USA.

A. Sandu, Department of Computer Science, Virginia Polytechnic Institute and State University, Blacksburg, VA 24061, USA.

J. H. Seinfeld, Departments of Chemical Engineering and Environmental Science and Engineering, California Institute of Technology, Pasadena, CA 91125, USA.

C.-H. Song, Department of Environmental Science and Engineering, Gwangju Institute of Science and Technology (GIST), 500-712 Gwangju, South Korea. (chsong@kist.re.kr)

D. G. Streets, Decision and Information Sciences Division, Argonne National Laboratory, Argonne, IL 60439, USA.

I. Uno, Research Institute for Applied Mechanics, Kyushu University, 816-8580 Fukuoka, Japan.

R. J. Weber, School of Earth and Atmospheric Sciences, Georgia Institute of Technology, Atlanta, GA 30332, USA.